Chapter 3

DFT-based synchrophasor estimation processes for Phasor Measurement Units applications: algorithms definition and performance analysis

Mario Paolone and Paolo Romano

Among the various logical components of a phasor measurement unit (PMU), the synchrophasor estimation (SE) algorithm definitely represents the core one. Its choice is driven by two main factors: its accuracy in steady state and dynamic conditions as well as its computational complexity.

Most of the SE algorithms proposed in the literature are based on the direct implementation of the Discrete Fourier Transform (DFT). This is due to the relatively low computational complexity of such technique and to the inherent DFT capability to isolate and identify the main tone of a discrete sinusoidal signal and to reject close-by harmonics. Nevertheless, these qualities come with non-negligible drawbacks and limitations that typically characterize the DFT: mainly they refer to the fact that the DFT theory assumes a periodic signal with time-invariant parameters, at least along the observation window. The latter, from one side should be as short as possible to be closer to the above-mentioned quasi-steady-state hypothesis also during power system transient; on the other hand, longer windows are needed when interested in rejecting and isolating harmonic and inter-harmonic signals that are quite frequent in power systems.

In this respect, this chapter first analyses the DFT with a particular focus on the origin of the well-known aliasing and spectral leakage effects. Then it formulates and validates in a simulation environment a novel SE algorithm, hereafter referred as iterative-Interpolated DFT (i-IpDFT), which considerably improves the accuracies of classical DFT- and IpDFT-based techniques and is capable of keeping the same static and dynamic performances independently of the adopted window length that can be reduced down to two cycles of signal at the nominal frequency of the power system.

This chapter is organized as follows: Section 3.2 introduces the nomenclature and some basic concepts in the field of synchrophasors. Section 3.3 presents the theoretical background of the DFT, with a specific focus on the detrimental effects of aliasing and spectral leakage. Next, Section 3.4 discusses advantages and drawbacks of DFT-based SE algorithms and derives the analytical formulation of the i-IpDFT method. Finally, Section 3.5, after illustrating the procedure presented in Reference 1 to assess the performances of a PMU, analyses the performances of the i-IpDFT

algorithm using two of the testing conditions presented in Reference 1 and compares them with those of the classical IpDFT technique.

3.1 Literature review

The scientific literature in the field of synchrophasor is quite recent but it already contains several contributions presenting novel algorithms for the calculation of phasors and/or local system frequency and rate of change of frequency (ROCOF).

In general, according to the adopted signal model, SE algorithms can be grouped into two categories [2]:

- algorithms based on a *static* signal model that assume that the waveform parameters are constant within the adopted window length;
- algorithms based on a *dynamic* signal model that assume a more sophisticated but generic signal model that includes also the possibility that the waveform parameters are time varying within the observation time window.

The main representatives of the latter category are based on the so-called Taylor–Fourier transform and were initiated with Reference 3. The advantages of these algorithms are evident and refer to the possibility of tracking and potentially estimating the power system dynamics (e.g., References 4, 5). Nevertheless, they are characterized by a non-negligible drawback, represented by their computational complexity that generally tends to be higher and does not typically match the available computational resources of standard hardware platforms. Additionally, it is barely impossible to track any kind of dynamics. In particular sudden ones, like those happening during faults, still deteriorate the quality of the estimated synchrophasor for the duration of the window length, that is typically quite high to keep the estimation uncertainty within reasonable limits.

On the other hand, SE algorithms based on a static signal model are the most common one, due to their good their trade-off between computational complexity and estimation accuracies. The majority of these methods is based on the direct implementation of the DFT [6]. Non-DFT-based SE methods based on a static signal model have also been proposed along the years. These include, among others, *zero-crossing methods* [7, 8], *demodulation filters* [7, 9], *adaptive filters* [10, 11], *compressive sensing* algorithms [12, 13], *wavelet*-based algorithms (e.g., Reference 14), *resampling* methods [15], *Prony*'s estimation methods [16] and *Matrix Pencil* methods [17].

Based on the window length, DFT-based SE algorithms can be grouped into multi-cycle, one-cycle or fractional-cycle DFT estimators performing recursive and non-recursive updates (e.g., References 18–20). In order to improve their accuracy, DFT-based algorithms have been sometimes proposed in combination with weighted least squares (e.g., Reference 21) or Kalman filter-based methods (e.g., Reference 22). Within this category, in order to reduce the effects of leakage and of the so-called picket-fence effect, the use of time windows in combination with the well-known Interpolated-DFT (IpDFT) technique has been first proposed in References 23, 24 and further developed in References 25–28. More in particular, contributions

[27, 28] have proven that the effects of long- and short-range leakage can be considerably minimized by adopting suitable windows functions and IpDFT schemes, respectively (see also References 29, 30). The advantages of this kind of approaches refer to the relatively simple implementation and low computational complexity capable of achieving reasonable accuracy and response times (RTs) after a careful selection of the algorithm parameters.

3.2 Definitions

This section recalls the theoretical definition of a *phasor* and derives the concept of *synchrophasor* starting from a given signal model. Then, it illustrates the general architecture of a PMU together with a preliminary analysis of its components.

3.2.1 Signal model

Electrical power is traditionally delivered from the generators to the end users through an infrastructure that is mainly composed by components operating in alternating current (AC). As a consequence, during normal operating conditions of the power system, voltage and current waveforms are usually modelled as signals characterized by a single sinusoidal component with constant parameters:

$$x(t) = A_0 \cdot \cos(2\pi f_0 t + \varphi_0) \tag{3.1}$$

being A_0 the nominal peak amplitude, φ_0 the initial phase, i.e., for $t = 0$, and f_0 the nominal frequency of the power system, i.e., 50 or 60 Hz.

However, even in normal operating conditions, a power system is never in a steady state. As a consequence, the parameters of (3.1) are rarely time-invariant and typically exhibit various *dynamics*. Frequency fluctuations are definitely the most evident phenomena and are typically related to changes in load or imbalances in generation and to the interactions between power demand in the grid, inertia of large generators and the operation of governors equipping the majority of power generators [31]. Additionally, when faults or other switching events take place, those variations can involve even larger frequency fluctuations [32].

Similarly, the waveform amplitude and phase are also affected by transient phenomena. Those can be relatively slow like in the case of power swings (i.e., amplitude and phase oscillations typically characterized by frequencies below few hertz) or faster like in the case of switching events or faults that usually produce step changes in voltage and current waveforms with spectral components that can even reach several hundreds of kilohertz.

Additionally, the main tone is often corrupted by other superposed signals that can be of different nature. In the literature, the following *interfering signals* are usually considered:

- *Harmonics*, namely spectral components at frequencies that are multiple integers of the AC system instantaneous frequency that, as previously stated, can be different from the nominal one (f_0). These signals are typically produced by power

electronics devices: in transmission systems, these can be flexible AC transmission systems (FACTS) or high-voltage direct current (HVDC) connections. On the other hand, at distribution level most of the harmonics are generated by converters typically interfacing distributed generation units or non-linear loads [31]. The literature on PMUs usually considers the effects of harmonics up to the 50th, assuming that higher frequency components are either attenuated by the analogue front-end filters of the PMU or too far in the frequency spectrum to be considered relevant [1].

- *Inter-* and *sub-harmonics*, namely spectral components at frequencies that are not multiple integers of the system frequency: inter-harmonics are characterized by a frequency that is bigger than the nominal one f_0 and sub-harmonics by a frequency that is smaller than f_0. The causes of inter- and sub-harmonics are usually static frequency converters, cycloconverters, subsynchronous converter cascades, induction motors, arc furnaces and all loads not synchronous with the fundamental power system frequency [33].
- Aperiodic components like *decaying direct current (DC) offsets* that are likely to appear during power system transients (consider, for instance, the case of a decaying short-circuit current or inrush of transformers/induction motors). The involved time constants can vary in the range between 0.1 and 10 s.
- *Wide-band noise* that includes both the "measurement noise" (namely the noise added by any measurement equipment) and the so-called grid noise. Regarding the latter, the most well-known phenomena are the thermal noise (also known as Johnson/Nyquist noise), the corona effect, and partial discharges. Both sources are usually modelled as a zero-mean Gaussian noise processes.

As a consequence, a generalized and more complete signal model that takes into account each one of the above-mentioned *dynamics* and *interfering signals* can be formulated as follows:

$$x(t) = A(t)\cos(2\pi f(t)t + \varphi_0) + \sum_{h=1}^{H} A_h(t)\cos(2\pi f_h(t)t + \varphi_h) + A_{DC}(t)e^{-\frac{t}{\tau}} + \epsilon(t) \tag{3.2}$$

where

- The first term represents the main tone of the spectrum, characterized by an instantaneous frequency $f(t)$ that is typically very close to the nominal frequency of the power system f_0, an instantaneous peak amplitude $A(t)$, and an instantaneous phase $\psi(t) = 2\pi f(t)t + \varphi_0$.[1]
- The second term models the contribution of any superposed sinusoidal tone excluding the main one. In other words, it includes all the effects of harmonic,

[1]The assumption of having a constant initial phase φ_0 is both mathematically and physically correct. It implies that the instantaneous phase variations are only due to the power system frequency variations and it avoids the possibility of having multiple couples of frequency and initial phase that produce the same instantaneous phase $\psi(t)$.

inter- and sub-harmonic tones, characterized by an instantaneous frequency $f_h(t)$ (that does not necessarily need to be an integer multiple of the fundamental frequency $f(t)$), peak amplitude $A_h(t)$ and instantaneous phase $\psi_h = 2\pi f_h(t)t + \varphi_h$, being φ_h the initial phase. During normal operating conditions, the peak amplitude is at least one order of magnitude lower than the one of the main tone $A(t)$, but no hypothesis can be made with respect to the instantaneous phase that does not necessarily have to match the one of the main tone.

- The third term models a decaying DC component characterized by an initial amplitude A_{DC} and an arbitrary time constant τ.
- The last element models a superposed wide-band noise that includes any other contribution not included in the previous terms.

3.2.2 Phasor

The phasor transformation has been historically adopted in electrical engineering to simplify the analysis of electrical systems in sinusoidal steady state. It consists in a one-to-one mapping between time-harmonic functions and complex numbers that can be adopted if and only if the instantaneous frequency f, peak amplitude A and initial phase φ are *time-invariant*, namely, if and only if the sinusoidal signal $x(t)$ is *stationary* (see (3.1)). In particular, such a transformation allows to represent a sinusoidal function of time like the one expressed by (3.1) with a single complex constant and vice versa. In order to derive it, we can rewrite (3.1) as:

$$x(t) = A \cdot \cos(2\pi ft + \varphi) \tag{3.3}$$

$$= \mathrm{Re}\{A \cdot e^{j(2\pi ft+\varphi)}\} \tag{3.4}$$

$$= \mathrm{Re}\{A \cdot e^{j\psi(t)}\} \tag{3.5}$$

where the dependency of $\psi(t)$ on time can be disregarded due to the stationarity of $x(t)$. We can then associate to the sinusoid $x(t)$ the complex number X and call it *phasor*:

$$x(t) \rightleftarrows X \triangleq A \cdot e^{j\psi} \tag{3.6}$$

$$= A \cdot [\cos(\psi) + j\sin(\psi)] \tag{3.7}$$

$$= X_r + jX_i \tag{3.8}$$

where the subscripts r and i identify the real and imaginary parts of X. A phasor can be represented either in polar (3.6) or rectangular (3.8) coordinates and the transformation from one set of coordinates to the other can be done using the well-known Euler identity (3.7).

3.2.3 Synchrophasor

The phasor concept cannot be directly applied to the analysis of a real AC power system for the simple reason that the *stationarity hypothesis* does not hold in practice. Nevertheless, even when the power system is not in steady state (e.g., during

electromechanical oscillations), the voltage and current variations can be assumed relatively slow and be treated as a series of steady-state conditions where the stationarity hypothesis holds (*quasi-steady-state* approximation).

With such an assumption the phasor analysis can be still applied but it requires that the measured values are referenced to a common time reference and taken at the same instant in time. For this reason the phasor concept has been extended to the *synchrophasor* one that has been first defined in the IEEE Std. 1344-1995 [34] as:

> [. . .] a phasor calculated from data samples using a standard time signal as the reference for the sampling process. In this case, the phasors from remote sites have a defined common phase relationship. [. . .]

Thanks to the explicit reference to a common time reference t, the synchrophasor concept allows to define a common phase relationship between phasors from remote sites. Additionally, it is not restricted to the analysis of stationary systems since a synchrophasor can be associated to any waveform characterized by a dominant sinusoidal component, also, during power system transients and with superposed interfering signals.[2]

The synchrophasor concept, and particularly the analytical definition of its phase, has been reviewed later in the IEEE Std. C37.118.1-2011 [1] that defined it as follows:

> [. . .] the instantaneous phase angle relative to a cosine function at the nominal system frequency synchronized to Coordinated Universal Time (UTC). [. . .] Under this definition ψ is the offset from a cosine function at the nominal system frequency synchronized to UTC. [. . .]

As shown in Figure 3.1, such a convention implies that, if a sinusoidal waveform representing a generic current or voltage, has its maximum at the UTC-second rollover (i.e., when the cosine has its maximum) the synchrophasor angle is 0°. It is 90° if the positive zero-crossing occurs at the UTC-second rollover.

The above IEEE Std. definition, which refers the phase to an hypothetical signal at the nominal frequency f_0 synchronized to the UTC, is restrictive and might generate ambiguities. A better and more generic definition of synchrophasor can be given by referencing both amplitude and phase estimations to the same time reference:

Definition . *The synchrophasor representation of the signal* $x(t)$ *in* (3.2) *is the complex function* $X(t)$ *characterized by an instantaneous amplitude and phase corresponding to the instantaneous amplitude* $A(t)$ *and phase* $\psi(t)$ *of the main tone of* $x(t)$*, respectively, being t the UTC time reference.*

[2]It is worth pointing out that the synchrophasor refers only to the main tone of $x(t)$ and does not take into account any other contribution that might be present in the original signal.

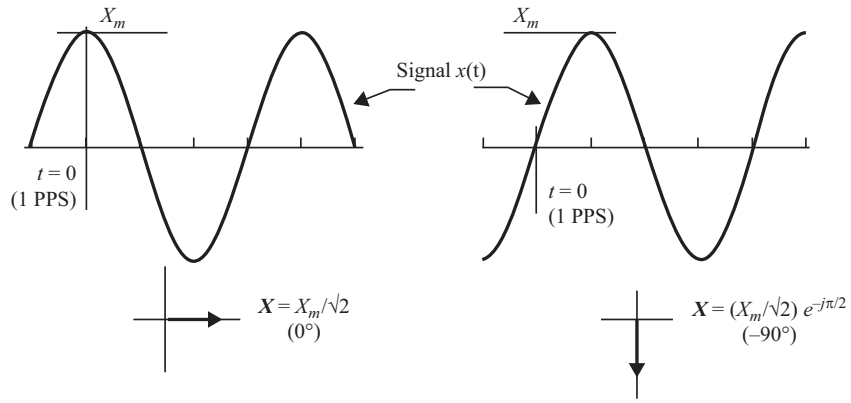

Figure 3.1 Phase convention for synchrophasors for a signal of amplitude X_m (adapted from Reference 1)

As a consequence, in the case of the signal $x(t)$ represented in (3.2), the associated synchrophasor is:

$$x(t) \rightleftarrows X(t) \triangleq A(t) \cdot e^{j\psi(t)} \tag{3.9}$$

$$= A(t) \cdot e^{j(2\pi f(t)t+\varphi)} \tag{3.10}$$

where $A(t)$ and $\psi(t)$ are the instantaneous peak amplitude and phase of the main tone of $x(t)$ (see (3.2)).

3.2.4 Frequency and rate of change of frequency

According to the IEEE Std. C37.118, frequency is defined starting from the first-order derivative of the instantaneous phase $\psi(t)$:

$$\frac{\mathrm{d}\psi(t)}{\mathrm{d}t} = \frac{\mathrm{d}}{\mathrm{d}t}[2\pi f(t)t + \varphi] \tag{3.11}$$

$$= 2\pi \left[f(t) + \frac{\mathrm{d}f}{\mathrm{d}t} t \right] \tag{3.12}$$

With the quasi-steady-state assumption, the term $\mathrm{d}f/\mathrm{d}t \approx 0$ and frequency can be defined as:

$$f(t) = \frac{1}{2\pi} \frac{\mathrm{d}\psi(t)}{\mathrm{d}t} \tag{3.13}$$

Similarly, the ROCOF is defined in the IEEE Std. C37.118 as the first-order derivative of the frequency:

$$ROCOF(t) = \frac{\mathrm{d}f(t)}{\mathrm{d}t} \tag{3.14}$$

It is worth underlying that the definitions given in (3.13) and (3.14) disagree as (3.13) has been obtained with an approximation ($\mathrm{d}f/\mathrm{d}t = 0$) that would lead to $ROCOF = 0$. However, for slow-varying frequencies (3.14) can be still considered as a correct approximation to compute the frequency time derivative.

3.2.5 Phasor measurement unit

According to the IEEE Std. C37.118.1-2011 [1], a PMU is a stand-alone physical unit or a functional unit within another physical unit

> [...] that produces synchronized phasor, frequency, and ROCOF estimates from voltage and/or current signals and a time synchronizing signal. [...]

The logic architecture of a generic PMU is shown in Figure 3.2. The PMU, in order to report synchronized measurements, needs to be equipped with a time-synchronization module capable of receiving the UTC absolute time from a reliable and accurate time source. The time-sync unit internally generates the "time base", namely a stable and accurate internal time reference, used by the signal conditioning and analog to digital (A/D) conversion unit to discipline[3] the sampling process of the input waveforms (as many as the number of connected input channels). The sampled waveforms are then transferred, sample by sample, to the SE algorithm, the core component of any PMU, that extracts the fundamental tone of a distorted sinusoidal waveform from a previously acquired set of samples and estimates its amplitude, phase and frequency, and ROCOF. The estimated values are then transferred to the data encapsulation and streaming unit that encapsulates and streams the data according, for instance, to the IEEE Std. C37.118.2-2011 [35] or IEC 61850-90-5 [36] data-transmission protocols.

It might be obvious, but still worth pointing out, that each one of the logical components highlighted in Figure 3.2 contributes to the global uncertainty that intrinsically characterizes the PMU estimations. In particular:

- The *time-sync unit*, depending on the adopted time source and dissemination technology, might deteriorate the synchronism of the sampling process (i.e., its alignment to the UTC-second rollover and the accuracy of the sampling time). Such an uncertainty can have non-negligible effects on the overall measurement accuracy, particularly in the estimation of the phase.[4] According to the PMU accuracy requirements dictated by Reference 1, the maximum acceptable timing uncertainty is $\pm 26\ \mu$s for a 60 Hz system and $\pm 31\ \mu$s for a 50 Hz system. In practice, PMUs adopt much more accurate timing sources, to further reduce the timing uncertainty.

[3]Such a functionality is quite common in PMUs but not mandatory. The synchronization of the sampling process to a common time reference can be also achieved by post-processing the acquired samples.
[4]The time-sync uncertainty linearly translates in phase uncertainty based on the instantaneous frequency values following the formula $\Delta\psi = 2\pi f \Delta t$, being $\Delta\psi$ and Δt the phase and time uncertainties.

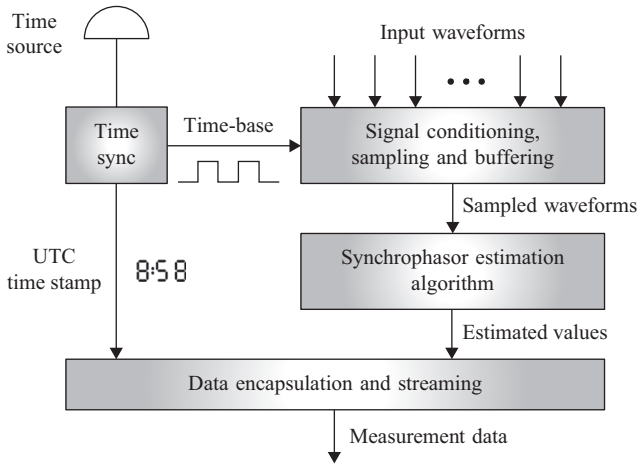

Figure 3.2 Scheme of a generic PMU

- The *signal conditioning and sampling unit* introduces an uncertainty that is mainly related to the intrinsic noise, non-linearities and gain errors introduced by the analogue filtering stage (anti-aliasing filters for instance) and to the quantization error introduced by the A/D converters.
- The *SE algorithm* is characterized by its own accuracy levels that are typically assessed in a simulation environment following the guidelines given by the IEEE Std. C37.118 [1] (see also Section 3.5). Nevertheless, this IEEE Std. does not take into account every possible power system operating condition and the SE algorithm estimations might be biased when processing non-contemplated waveforms. For instance, it has already been demonstrated that different SE algorithms might produce different estimations, particularly when exposed to power system transients [37].

Finally, it should be noted that, in order to transform the power system voltage and current waveforms to levels appropriate for the PMU analogue front-end, the PMU must be interfaced to the electrical grid using instrument transformers (refer to Reference 38 for a partial review of the available instrument transformer technologies).

Although this aspect will not be treated along this chapter, it is worth pointing out that the uncertainty introduced by this transformation stage, if not properly designed, might be dominant and exceed those introduced by the PMU components. For instance, in the case of standard magnetic core voltage and current transformers (VTs and CTs), their accuracy is generally limited to class 0.5. This, according to the definition of the standards [39, 40], translates, at full scale, to a maximum ratio error of 0.5% and a maximum phase error of 6 mrad for VTs and 9 mrad for CTs. Such

an uncertainty, in most of the cases, exceeds the one of the PMU and deteriorates, therefore, the expected accuracies.

3.3 The discrete Fourier transform

The DFT is the most common analytical tool to extract the frequency content of a finite and discrete sequence of samples, obtained from the periodic sampling of a continuous waveform in the time domain. This also applies to the field of synchrophasors, where, as it will be shown later, the DFT represents the most common technique to extract the waveform parameters out of a sequence of samples.

In this respect, this section derives the analytical formulation of the DFT starting from the theoretical formulation of the Fourier transform of a continuous signal of infinite duration. Next, it highlights the most relevant DFT properties and investigates two well-known effects caused by the computation of the DFT such as *aliasing* and *spectral leakage*.

3.3.1 From the Fourier transform to the DFT

The Fourier transform of a continuous function of time $x(t)$, satisfying integrability constraints [41] is defined as:

$$X(f) = \int_{-\infty}^{+\infty} x(t)e^{-j2\pi ft}\mathrm{d}t \tag{3.15}$$

and it is used to transform a continuous time-domain function $x(t)$ to a continuous frequency-domain function $X(f)$.

In practice, continuous signals are sampled using A/D converters producing a sequence of samples $x(n)$ that can be easily treated by any digital hardware (samples are assumed to be equally spaced by $T_s = 1/F_s$, being F_s the PMU sampling rate). In this respect, the discrete-time Fourier transform (DTFT) has been defined to transform a time-domain sequence of infinite length $x(n),\ n \in \mathbb{N}$ into a continuous frequency-domain function $X(f)$ according to the following equation [6]:

$$X(f) = \sum_{n=-\infty}^{\infty} x(n)e^{-j2\pi fn} \tag{3.16}$$

Such a transformation cannot be applied to the analysis of real signals, as it assumes the possibility to calculate a continuum of functional values $X(f)$ by means of an infinite summation that is unfeasible in digital computers.

A more practical transformation is represented by the so-called discrete Fourier series (DFS), a frequency analysis tool conceived for periodic sequences of infinite length $\tilde{x}(n)$ characterized by period N. The DFS can be seen as a frequency-discretized version of the DTFT [6] and it involves a finite summation of N complex terms:

$$\widetilde{X}(k) = \sum_{n=0}^{N-1} \tilde{x}(n)e^{-j\frac{2\pi kn}{N}}, \qquad 0 \le k \le N-1 \tag{3.17}$$

In particular, the DFS differs from the DTFT in that its input and output sequences are both finite; it is therefore said to be the Fourier analysis of periodic discrete-time functions.

When the DFS is used to represent a generic (i.e., not necessarily periodic) finite-length sequence of samples $x(n)$, $n \in [0, N-1]$, it is called the DFT that is defined as follows:

$$X(k) \triangleq \frac{2}{B} \sum_{n=0}^{N-1} w(n)x(n)W_N^{kn}, \qquad 0 \leq k \leq N-1 \tag{3.18}$$

where $w(n)$ is a discrete windowing function used to extract a portion of the infinite length original sequence (see Section 3.3.4.3 for further details about windowing functions),

$$B \triangleq \sum_{n=0}^{N-1} w(n) \tag{3.19}$$

is the DFT normalization factor and

$$W_N \triangleq e^{-j2\pi/N} = \cos(2\pi/N) - j\sin(2\pi/N), \qquad W_N^{kN} = 1, k \in \mathbb{N} \tag{3.20}$$

is the so-called *twiddle factor*.

The DFT spectrum can be equivalently expressed in matrix form for a more intuitive understanding of its logic:

$$\begin{bmatrix} X(0) \\ X(1) \\ \vdots \\ X(k) \\ \vdots \\ X(N-1) \end{bmatrix} = \begin{bmatrix} 1 & 1 & 1 & \cdots & 1 \\ 1 & W_N & W_N^2 & \cdots & W_N^{N-1} \\ \vdots & \vdots & \vdots & & \vdots \\ 1 & W_N^{(k)_N} & W_N^{(2k)_N} & \cdots & W_N^{((N-1)k)_N} \\ \vdots & \vdots & \vdots & & \vdots \\ 1 & W_N^{N-1} & W_N^{N-2} & \cdots & W_N \end{bmatrix} \begin{bmatrix} x(0) \\ x(1) \\ \vdots \\ x(k) \\ \vdots \\ x(N-1) \end{bmatrix} \tag{3.21}$$

where $(\cdot)_N$ identifies the mod$N$ operator. It is easy to show that the columns of matrix $[W_N^{kN}]$ of (3.21) are linearly independent. Therefore, they are a base of $\mathbb{C}^N$.

3.3.2 DFT interpretation and relevant properties

The DFT is a sequence of complex values that are equally spaced in the frequency spectrum and represent, under specific conditions, a portion of the Fourier transform of the original continuous-time signal $x(t)$ (see Section 3.3.3 for further details about the original assumptions to guarantee an exact matching between the DFT and the Fourier transform). It is the result of a frequency decomposition of the finite-length discrete signal that is projected onto the sinusoidal basis set W_N^{kn}, $0 \leq k \leq N-1$.

In order to correctly interpret the DFT spectrum obtained by applying (3.18) to a generic real-valued finite sequence $x(n)$, some considerations must be made.

3.3.2.1 DFT periodicity

As shown in Section 3.3, the DFT of a finite sequence of real values $x(n)$ is a finite sequence of complex values $X(k)$ (also called "bins") defined in the interval $0 \leq k \leq N-1$. This does not mean that the DFT cannot be computed outside of the interval $0 \leq k \leq N-1$, but simply that this will result into a periodic extension of $X(k)$ due to the periodicity of the theoretical spectrum of the sampled signal.

Usually, when analysing signals through the DFT, the convention is to associate the DFT bins in the interval $0 \leq k \leq N/2-1$ to the "positive" frequencies $0 \leq f \leq F_s/2$ and the bins in the interval $N/2 \leq k \leq N-1$ to the "negative" frequency range $F_s/2 \leq f < 0$ (see also Figure 3.4(b)).

3.3.2.2 DFT symmetry

The DFT of a real-valued sequence is symmetric. In particular, the DFT bins in the interval $0 \leq k \leq N/2-1$ (positive frequency range) are related to those in the interval $N/2 \leq k \leq N-1$ (negative frequency range) based on the following equivalences:

$$\begin{cases} X(k) = X^*((k)_N) \\ \mathrm{Re}\,(X(k)) = \mathrm{Re}\,(X((-k)_N)) \\ \mathrm{Im}\,(X(k)) = -\,\mathrm{Im}\,(X((-k)_N)) \\ |X(k)| = |X((-k)_N)| \\ \angle X(k) = -\angle X((-k)_N) \end{cases} \tag{3.22}$$

As a consequence, when applying the DFT to real-valued signals, each frequency component will appear twice in the DFT spectrum: once in the positive frequency range (the so-called *positive image*) and once in the negative frequency range (the so-called *negative image*).

3.3.2.3 DFT frequency discretization

According to (3.18), the DFT of the sequence $x(n)$, $n \in [0, N-1]$, provides samples of the DTFT at N equally spaced discrete frequencies. In particular the kth DFT bin represents the frequency content of the original signal at the normalized frequency $2\pi k/N$ as it is the result of the projection of the finite-length sequence into the basis vector characterized by that frequency (see (3.18)). As a consequence, consecutive bins are separated by the normalized frequency interval $2\pi/N$ and the whole DFT spectrum will cover the normalized frequency interval $[0, 2\pi]$ or equivalently, due to the DFT periodicity, $[-\pi, \pi]$.

In order to derive a more practical scale for the DFT frequency axis, it should be noted that the finite-length sequence $x(n)$ is associated to specific instants in time according to the adopted sampling rate F_s. Therefore, based on the sampling rate, the window length can be expressed as a function of time as $T = N/F_s$ and, accordingly, each basis vector W_N^{kn} can be referred to an absolute frequency. In particular, the bin for $k = 0$ can be associated to the DC component ($f = 0$), the bin for $k = 1$ to a frequency $f = 1/T$ and a generic kth bin to a frequency $f = k/T$. It is then clear that the frequency separation between two consecutive bins is $\Delta f = 1/T$ and

can only be increased at the price of enlarging the window length T. On the other hand, the frequency range that can be represented with the DFT of the finite-length sequence $x(n)$ obtained by sampling the original signal $x(t)$ with a sampling rate F_s is $[-F_s/2, F_s/2]$.

3.3.3 DFT effects

The DFT is often improperly considered as a "sampled" version of the continuous Fourier transform. This statement is valid only if both of the following assumptions are satisfied:

- the original signal $x(t)$ can be perfectly reconstructed from the discrete sequence of samples $x(n)$;
- the original signal $x(t)$ is periodic and characterized by a period that is contained an integer number of times in the chosen window length T.

In general, these hypotheses do not always hold and, as demonstrated in Section 3.3.1, the DFT can be correctly interpreted only from a precise knowledge of the theoretical background of the Fourier analysis. In this respect, Figure 3.3 shows the necessary steps required to analyse a continuous-time signal $x(t)$ with the DFT. The first step is represented by the continuous-to-discrete-time conversion that allows to transform the original continuous signal into an equivalent sequence of samples $x(n)$. This is typically performed by an A/D converter that, for the time being, is considered to be ideal; in other words, it is assumed to produce a sequence of equally spaced samples that are equal to the original signal evaluated at regular time intervals $x(n) = x(nT_s)$, being $T_s = 1/F_s$ the sampling time as introduced before. The A/D conversion process produces an infinite sequence of samples that, in order to be processed by the DFT, needs to be clustered in finite portions containing the same number of samples N. This is done by applying to the infinite sequence $x(n)$ a finite duration windowing function $w(n)$. After this steps the DFT can be applied to each portion of the sampled signal.

In what follows, each one of the above-mentioned steps is analytically modelled and analysed using the Fourier transform theory. This will help understanding the previously mentioned assumptions and derive the two main DFT error sources, namely, *aliasing* and *spectral leakage*.

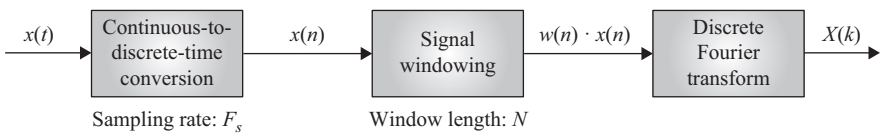

Figure 3.3 Main steps to apply a DFT-based digital signal processing technique to a continuous-time signal $x(t)$

3.3.3.1 Aliasing

As known, the sampling process can be modelled as the multiplication of the input continuous signal $x(t)$ with a periodic impulse train $s(t)$ [6]:

$$x_s(t) = x(n \cdot T_s) = x(t) \cdot s(t) \tag{3.23}$$

$$= x(t) \cdot \sum_{n=-\infty}^{\infty} \delta(t - nT_s) \tag{3.24}$$

$$= \sum_{n=-\infty}^{\infty} x(nT_s) \cdot \delta(t - nT_s) \tag{3.25}$$

being δ the unit *impulse function* or *Dirac delta function*.

The frequency-domain representation of this transformation can be given by applying the Fourier transform theory and properties to (3.24). In particular, by recalling that the Fourier transform of the product of two functions is the convolution of the Fourier transforms $\mathfrak{F}$ of the two functions, the Fourier transform of the sampled signal can be analytically derived as follows:

$$x_s(t) = x(t) \cdot \sum_{n=-\infty}^{\infty} \delta(t - nT_s) \xrightarrow{\mathfrak{F}} X_s(f) = X(f) * \frac{1}{T_s} \sum_{k=-\infty}^{\infty} \delta\left(f - \frac{k}{T_s}\right) \tag{3.26}$$

$$= \frac{1}{T_s} \sum_{n=-\infty}^{\infty} X\left(f - \frac{k}{T_s}\right) \tag{3.27}$$

where, to obtain (3.27), we have taken advantage of the property that the convolution between a Dirac δ function and any generic function is the value of the generic function evaluated at the location of the Dirac δ function.

As a consequence, the Fourier transform of the sampled signal is composed by infinite copies of the spectrum $X(f)$ (see Figure 3.4(a)) of the original continuous signal $x(t)$. These copies are shifted by integer multiples of the sampling frequency $F_s = 1/T_s$ and, then, superimposed to produce the periodic Fourier transform depicted in Figure 3.4 for a band-limited original spectrum characterized by a bandwidth F_m and a sampling rate F_s.

From Figure 3.4(b) it is evident that, if the signal is band limited with bandwidth $F_m < F_s/2$, the spectrum copies are not overlapping and the original spectrum $X(f)$ can be reconstructed by low-pass filtering the base-band copy of the spectrum $X_s(f)$. On the other hand, if this is not the case and the bandwidth F_m of the original signal is higher than half of the sampling rate F_s (i.e., $F_m > F_s/2$), the spectrum copies are overlapping so that when they add together, the original spectrum $X(f)$ is no longer recoverable by low-pass filtering (see Figure 3.4(c)).

The latter phenomenon is called *aliasing* and it results into a distortion of the original signal that cannot be any longer be reconstructed from the sampled signal. Such a phenomenon is the basis of the well-known Nyquist–Shannon sampling theorem [6]:

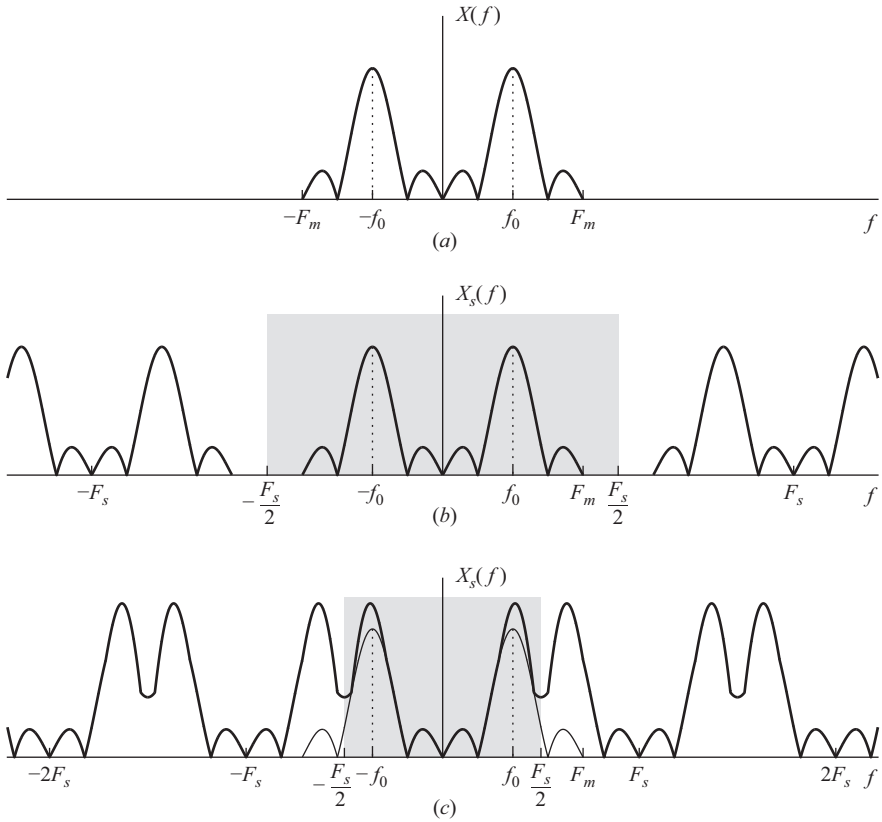

Figure 3.4 Effects of aliasing for a signal characterized by a main frequency component at f_0 and a bandwidth F_m, sampled with a sampling rate F_s. The figure shows, in order, the Fourier transforms of the continuous-time signal (a) and the Fourier transform of the sampled signal with a sampling rate respecting (b) or violating (c) the Nyquist–Shannon theorem

Theorem 3.1 (Nyquist–Shannon). *Let $x(t)$ be a band-limited signal and $X(f)$ its Fourier transform with*

$$X(f) = 0, \qquad f > F_m$$

Let $x(n) = x(nT_s)$ ($n \in \mathbb{N}$) be an infinite sequence of equally spaced samples obtained by sampling the continuous signal $x(t)$ with a sampling frequency $F_s = 1/T_s$. Then $x(t)$ is uniquely determined by the sequence of samples $x(n) = x(nT_s)$ if

$$F_s > 2F_m$$

In other words, in order to be able to correctly reconstruct the signal $x(t)$ from the infinite sequence of samples $x(n)$, the original signal must be sampled at a sampling

rate F_s that must be at least two times higher than the maximum frequency component contained in the original spectrum $X(f)$.

3.3.3.2 Spectral leakage

Once the original continuous signal $x(t)$ has been sampled, it must be clustered in portions to be analysed by the DFT. This process is called *windowing* and consists in multiplying the infinite sequence of samples $x(n)$ by a specific windowing function $w(n)$ (see Figure 3.5).

In order to derive the effects of windowing, let us consider, without loss of generality, a signal $x(t)$ that is only composed by a sinusoidal component at the nominal frequency of the power system f_0:

$$x(t) = A\cos(2\pi f_0 t) \tag{3.28}$$

As known, its Fourier transform is simply:

$$X(f) = \frac{A}{2}\left[\delta(f - f_0) + \delta(f + f_0)\right] \tag{3.29}$$

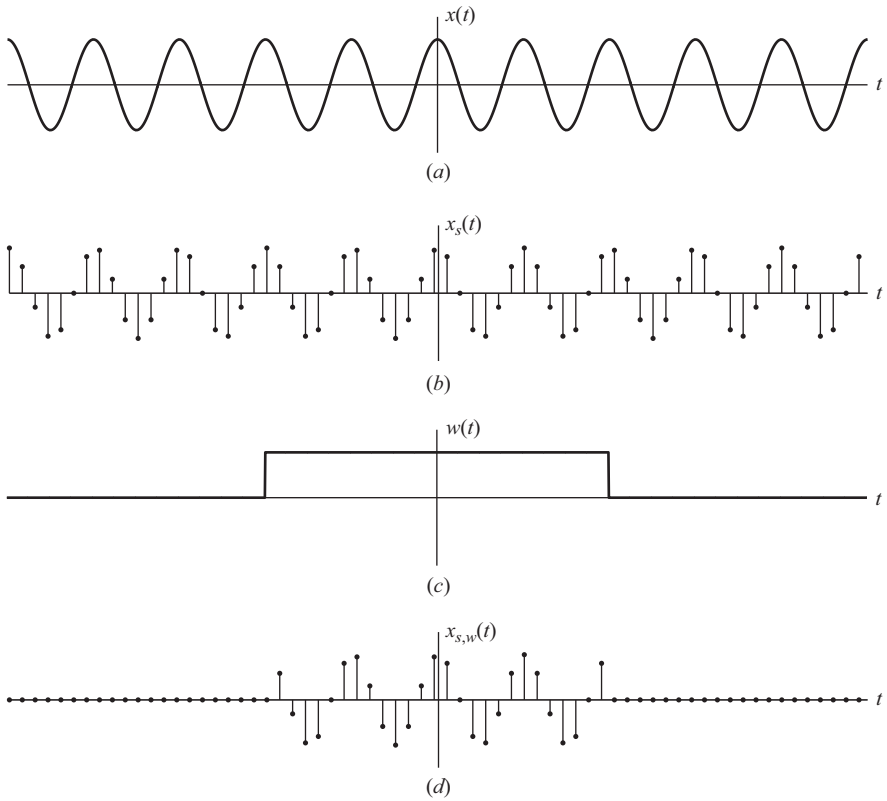

Figure 3.5 Successive applications of sampling and windowing to obtain a portion of samples of the original input signal $x(t)$. The figure shows, in order, (a) the continuous-time signal $x(t)$, (b) the sampled signal $x_s(t)$, (c) the rectangular windowing function $w(t)$ and (d) the sampled and windowed signal $x_{s,w}(t)$

The windowing operation can be modelled as the multiplication between the sampled sinusoidal signal $x_s(t)$ and the adopted window function $w(t)$ (see Figure 3.5):

$$x_{s,w}(t) = w(t) \cdot x_s(t) = w(t) \cdot [x(t) \cdot s(t)] \tag{3.30}$$

$$= [w(t) \cdot x(t)] \cdot s(t) \tag{3.31}$$

$$= [w(t) \cdot A\cos(2\pi f_0 t)] \cdot \sum_{n=-\infty}^{\infty} \delta(t - nT_s) \tag{3.32}$$

By recalling that (i) the Fourier transform of the product between two functions equals the convolution between the Fourier transform of each one of the two functions and (ii) the convolution between a Dirac δ function and any generic function is the value of the generic function evaluated at the location of the Dirac δ function, the Fourier transform of $x_{s,w}(t)$ can be computed as:

$$x_{s,w}(t) \xrightarrow{\mathfrak{F}} X_{s,w}(f) = [W(f) * X(f)] * S(f) \tag{3.33}$$

$$= \frac{A}{2}[W(f - f_0) + W(f + f_0)] * \frac{1}{T_s}\sum_{k=-\infty}^{\infty} \delta\left(f - \frac{k}{T_s}\right) \tag{3.34}$$

$$= \frac{A}{2T_s}\sum_{n=-\infty}^{\infty}\left[W\left(f - \frac{k}{T_s} - f_0\right) + W\left(f - \frac{k}{T_s} + f_0\right)\right] \tag{3.35}$$

In other words, the spectrum of the sampled and windowed signal $x_{s,w}(t)$ is composed by infinite copies of the spectrum of the windowed signal $W(f) * X(f)$ shifted by integer multiples of the sampling rate $F_s = 1/T_s$ and, then, superimposed.

In order to illustrate the effects of leakage on the DFT, let us consider just the base-band copy of the spectrum of $X_{s,w}(f)$ for $k = 0$. Additionally, let us adopt the simplest windowing function, namely the rectangular one.[5] The Fourier transform of the rectangular window is the so-called *sinc function* (see Figure 3.6(a))

$$\text{sinc}(fT) = \frac{\sin(\pi fT)}{\pi fT} \tag{3.36}$$

that is characterized by the peculiar property:

$$\text{sinc}(fT)|_{f=\frac{1}{T}} = 0 \tag{3.37}$$

namely, the zero-crossing of the Fourier transform of the rectangular window is equally spaced and happens at integer multiples of $1/T$.

According to (3.35), the base-band copy of the Fourier transform of $X_{s,w}(f)$ will be composed by two sinc functions centred around $\pm f_0$. In case f_0 is a multiple of the DFT frequency resolution $\Delta f = 1/T$ (i.e., if the window contains an integer number

[5]Nevertheless, such an analysis can be made with any other kind of window (see Section 3.3.4.3 for further details about the various type of windowing functions).

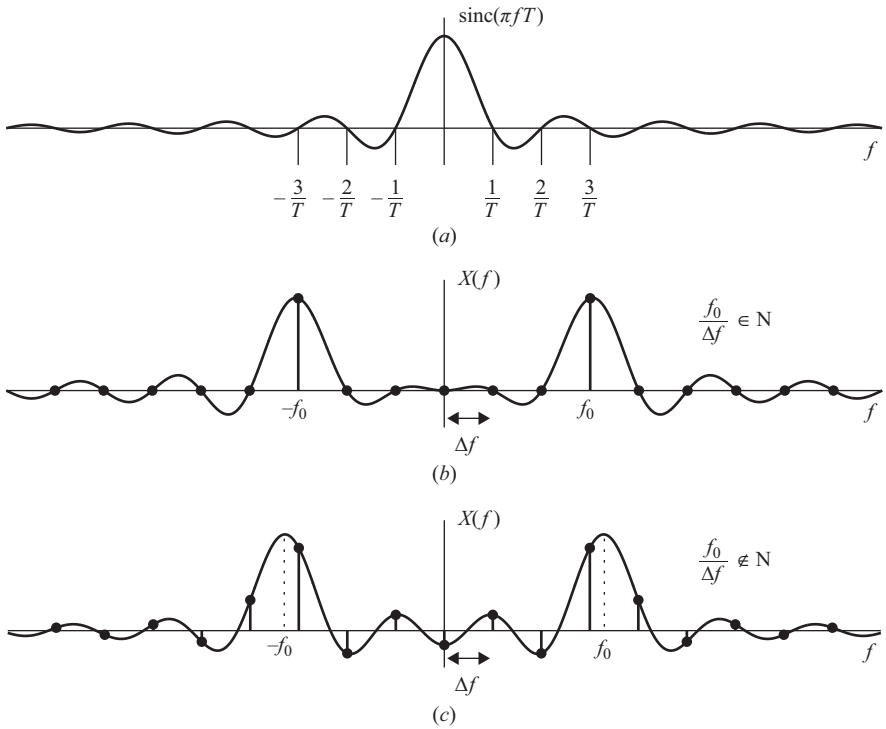

Figure 3.6 Graphical representation of the spectral leakage effects on the Fourier Transform (continuous line) and the DFT (black dots) when using a rectangular window of length T to analyze a sinusoidal signal characterized by a main tone at f_0. In (a) the sinc function is depicted. In (b) the effects of leakage are not visible since the adopted window contains an integer number of periods of the input signal; they appear in (c) where the adopted window length is not a multiple of the period of the input signal

of periods of the signal), the zero-crossings of the translated sinc functions happen exactly at multiples of $1/T$. The only frequency that will have a non-zero projection into the DFT basis set will be $f = \pm f_0$ (i.e., the DFT bin with index $k = f_0/\Delta f$) and the resulting DFT will be characterized by only two non-zero bins, at index $\pm k$ (see Figure 3.6(b)).

On the other hand, if f_0 is not a multiple of the frequency resolution Δf (i.e., if the window does not contain an integer number of periods of the signal), the zero-crossings of the translated sinc functions do not happen exactly at multiples of $1/T$. Therefore, all the discrete frequencies will exhibit non-zero projections on the DFT basis set even though the majority of the spectrum energy will still be concentrated around $f = f_0$ (see Figure 3.6(c)).

This effect is the so-called *spectral leakage* and it evidently arises when the sampling process is not synchronized with the fundamental tone of the signal under

analysis and the DFT is computed over a non-integer number of cycles of the input signal. As it will be discussed later, spectral leakage can be separated into *short-term* and *long-term* spectral leakage: the first refers to the effects of the main lobe width of the Fourier transform of the adopted window that can cause difficulties in identifying the "true" maximum of a specific portion of the DFT spectrum. The latter, on the other hand, refers to the effect caused by the side lobes (i.e., the "tails") of the Fourier transform of the adopted window that can generate the so-called spectral interference between nearby tones.

3.3.3.3 Spectral sampling

As shown before, the DFT of the sequence $x(n)$, $n \in [0, N-1]$, provides samples of the DTFT of the equivalent windowed signal, at N equally spaced discrete frequencies $f_k = k \cdot \Delta f = k/T$, being $-N/2 \leq k \leq N/2 - 1$ (see Figure 3.6). In Section 3.3.3.2, we have shown how such a reduced frequency resolution can turn out to be beneficial when the input signal $x(n)$ is composed by a single tone and sampled coherently with respect to its frequency (i.e., when $F_s = k \cdot f_0$, being F_s and f_0 the sampling rate and the main-tone frequency, respectively). Nevertheless, coherent sampling is purely ideal and the DFT energy is spread along the whole spectrum. Consequently, the DFT bin values and the frequency axis discretization change based on the adopted number of samples N and window length T.

In general, when the target is identifying the parameters of a signal, the frequency resolution Δf plays a major role as it defines the accuracy in locating the correct position in the frequency spectrum of the tone under analysis. As we will see later, the IpDFT method will partially overcome such a limitation with a proper interpolation of the DFT bins.

3.3.4 DFT parameters

The DFT output can be modified by acting on three main parameters: the sampling rate F_s, the window length T, and the window profile $w(n)$. Together, they determine the amount of aliasing and spectral leakage and the frequency resolution of the DFT.

3.3.4.1 Sampling rate

The sampling rate F_s defines the frequency range that can be correctly analysed with the DFT. It is limited on one side by the Nyquist–Shannon sampling theorem (see Section 3.3.3.1) and on the other side by the hardware limitations of the platform where the DFT has to be implemented. In particular, in the real world, F_s is limited by the maximum and possible sampling rates of the adopted A/D conversion technology and by the processing and data storage capabilities of the processing unit (the higher the sampling rate the higher the amount of samples to be processed in real time by the DFT).

3.3.4.2 Window length

The window length is the most critical parameter when analysing the frequency content of a finite sequence of samples through the DFT. Its selection depends on the specific

field of application and it is typically chosen as a trade-off between the required frequency resolution and the desired bandwidth.

According to what stated in the previous sections, the window length T defines the DFT frequency resolution $\Delta f = 1/T$ that determines the uncertainty to correctly identify the position of a tone and, therefore, the uncertainty in identifying its parameters. In Section 3.3.3.2, we have also shown how the window length T influences the frequency separation between the zero-crossings of the sinc function. This, in turn, determines the main lobe width, namely the DFT capability to detect nearby tones, and the side-lobes decaying rate, namely the amount of spectral interference produced by each tone of the spectrum. In general, the longer the window length T, the higher the possibility to detect nearby tones and the lower the effects of the spectral interference produced by near-by tones (see Figure 3.7). Nevertheless, the higher the window length the more probable the possibility that the waveform parameters within the window length are not constant at that therefore the DFT assumptions are not respected, introducing therefore an inherent error in the DFT spectrum.

In this respect, it is worth pointing out that the window length T is a crucial parameter when applying the DFT to SE. As defined in Reference 1 (see also Section 3.5.1.3), the RTs and measurement reporting latencies are two very important characteristics of a PMU that are mainly influenced by the adopted window length. In general, the lower the window length, the lower the RT and measurement reporting latencies and therefore the higher the possibility to use the PMU for specific applications that require fast response and reduced latencies (e.g., power system protections).

Last but not least, it should be observed that the window length T determines, together with the sampling rate F_s, the number of samples $N = T/F_s$ to be processed by the DFT. Even though this is usually forgotten, the number of samples is an important parameter when processing waveforms corrupted by white noise. As shown

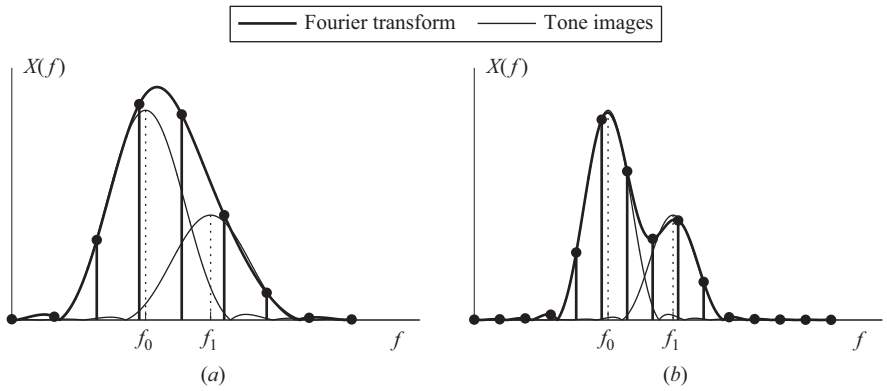

Figure 3.7 Effects of the window length on the detectability of a nearby tone characterized by a frequency f_1 and half of the amplitude of the main tone at f_0. In panel (a), a shorter window length does not allow to detect the tone at f_1 whereas this is possible in panel (b) where a longer window length is adopted

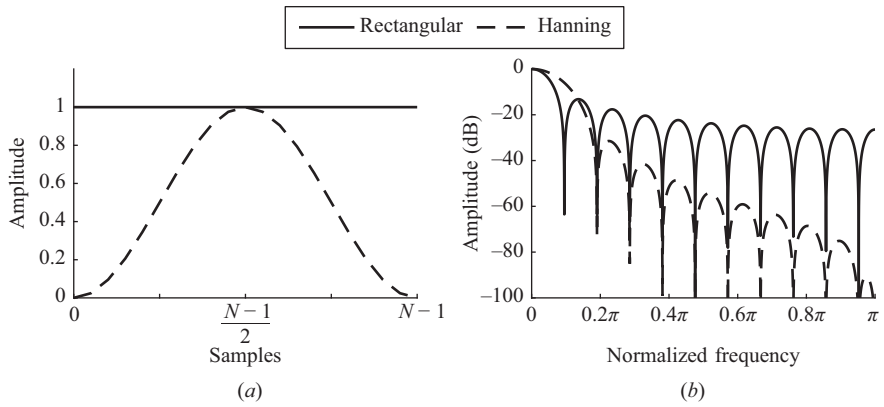

Figure 3.8 Comparison between the time and frequency profiles of the rectangular (continuous line) and the Hanning (dashed line) window

in Reference 31, the effects of white noise on the DFT uncertainty can be effectively reduced by increasing the number of samples to be processed.

3.3.4.3 Window profile

In Section 3.3.3.2, it has been shown that spectral leakage arises when the input signal is not periodic within the window length. This has been demonstrated in the case of a rectangular window function but the proposed analysis could be extended to any kind of windows. Nevertheless, the spectral leakage effects might be reduced by adopting specific windowing functions.

As shown in Reference 29, the characteristics of a window function can be expressed in terms of several metrics. For our purposes we can restrict the analysis to:

- the *main lobe width*, namely, the width of the highest lobe of the adopted window (see Figure 3.6 in the case of a rectangular window), that is typically measured by evaluating the −3 dB bandwidth of the Fourier transform of the adopted window;
- the *side-lobe levels* and *decaying rate*, namely, the relative height of the second, third, etc. lobes with respect to the height of the main one and their characteristic decaying rate.

Whereas both parameters impact the tone detectability, namely the capability to detect two nearby tones through DFT, the latter is also responsible of the aforementioned spectral interference, namely the detrimental effect that neighbouring tones produce on the main tone under analysis. This effect is quite noticeable when using a rectangular window (see Figure 3.8) that, besides being the windowing function with the minimum main lobe width, it is characterized by the highest side lobes (see Reference 29 for a detailed analysis of the window parameters). To improve this characteristic, Harris in Reference 29 has first derived a set of bell-shaped windowing functions that, by reducing the discontinuities at the edge of a window, reduce the side-lobe levels. Unfortunately, this comes at the price of enlarging the main lobe width and, therefore, reducing the tone detectability (see Figure 3.8).

3.3.5 DFT calculation in real time

If not properly designed and implemented, the DFT calculation might represent a considerable bottleneck when running a DFT-based SE algorithm in a real-time environment. As discussed in Section 3.5.1.3, it also affect both measurement reporting latencies and achievable reporting rates. Indeed, particularly when the DFT is calculated over a discrete sequence of samples obtained with a sampling rate of some tens of kilohertz, the high number of samples within a single observation window makes the DFT calculation according to (3.18) computationally intensive. This, combined with the maximum reporting rate and measurement latency requirements defined in Reference 1, makes the development of a PMU based on the DFT, a quite challenging task.

In this respect, in order to improve both latencies and throughput, several efficient techniques to compute the DFT spectrum have been proposed in the literature. They can be separated into two main categories: *recursive* and *non-recursive* algorithms.

Within the group of non-recursive algorithms the well-known *fast Fourier transform* (FFT) algorithm (e.g., Reference 42) is widely used. Typically, this implementation is adopted to perform harmonic analysis over an extended portion of the spectrum even though its deployment on embedded system is usually onerous. When, on the other hand, only a subset of the overall DFT spectrum is used to estimate the synchrophasor (see for instance Reference 24), the so-called *short-time Fourier transform* (STFT) turns out to be very effective [6]. In both cases, the measurement reporting latencies are proportional to the amount of samples to be processed. As a consequence, the algorithm throughput can only be improved at the cost of deteriorating the PMU accuracy levels. The first option is to reduce the sampling rate and eventually originate aliasing (see Section 3.3.3.1); the other one refers to the adoption of shorter window lengths and potentially increase the spectral leakage effects (see Section 3.3.3.2).

In order to increase the throughput without decreasing the precision of the adopted DFT-based SE algorithm, DFT can be calculated via recursive algorithms that are usually characterized by a lower number of operations to update the values of a single DFT bin (e.g., Reference 31). Despite this evident advantage with respect to the class of non-recursive DFT algorithms, the two categories do not generally have identical performances. In particular, the majority of the recursive algorithms suffers of errors due to either the approximations made to perform the recursive update, or the accumulation of the quantization errors produced by the finite word length of computers [43].

A very effective method for sample-by-sample DFT bins computation is represented by the so-called sliding-DFT (SDFT) technique presented in Reference 44. This reference demonstrates the efficiency of this method in comparison with the popular Goertzel algorithm and its computational advantages over the more traditional DFT and FFT, but also its drawbacks. Unfortunately, the approach proposed in Reference 44 is only marginally stable. In particular, if the truncation errors on the computation of the filter coefficients are not severe, the SDFT is bounded-input, bounded-output stable. Otherwise, the algorithm suffers from accumulated errors

Table 3.1 Characteristic computational complexity and numerical stability of the STFT, SDFT (stable and unstable version) and MSDFT methods (M is the number of samples within a window of length T)

Method	Computational workload		Numerical stability
	ADD	MUL	
Short-time Fourier transform (STFT)	M	M	✓
Sliding DFT (SDFT)	4	4	✗
Guaranteed-stable SDFT (rSDFT)	5	4	✓
Modulated sliding DFT (MSDFT)	10	7	✓

and is, consequently, potentially unstable. Whereas common approaches found in the literature [44, 45] face this problem compromising results accuracy for guaranteed stability, the method proposed in Reference 46 and called modulated sliding DFT (MSDFT) is guaranteed stable without sacrificing accuracy.

In what follows, three of the most efficient techniques to compute a portion of the DFT spectrum, namely, the STFT, SDFT and MSDFT, will be presented and analysed with respect to their precision and computational complexity (see also Table 3.1).

3.3.5.1 Short-time Fourier transform

Starting from what formulated in (3.18), the DFT can be potentially updated every time-step n, based on the most recent set of samples $\{x(n-N+1), x(n-N+2), \ldots, x(n)\}$, according to the following time-dependent equation:

$$X_k(n) = \sum_{m=0}^{N-1} x(q+m) \cdot W_N^{-km} \tag{3.38}$$

being N the number of samples within the window of length T, n the time-step index, k the DFT-bin index, $q = n - N + 1$, and $W_N^{-km} = e^{-j2\pi km/N}$ the DFT complex twiddle factor.

The derived equation is the so-called STFT, namely the simplest technique to apply the DFT theory to a real signal. It assumes to split the signal into partially overlapping block of samples of equal length N and apply the DFT computation independently to each one of them. Consequently, such a calculation is extremely inefficient: although two consecutive estimations are derived from a partially overlapping windows, in order to update the DFT estimation, it assumes to re-process already analysed portions of the signal. Nevertheless, such a technique can still be applied to SE, as long as the PMU does not need to report estimated data too frequently and the adopted hardware platform has enough available computational resources to host a parallel computation of the DFT, according to (3.38), over the whole set of input channels.

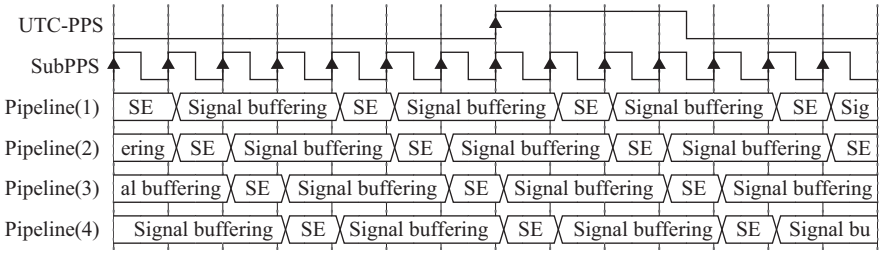

Figure 3.9 Digital timing diagram of a hypothetical PMU that estimates synchrophasors 50 times per second using the STFT technique. A four-stage pipeline is here adopted to achieve the desired reporting rate with a three-cycle window to calculate the DFT and estimate the synchrophasor (SE stands for synchrophasor estimation)

For instance, in order to achieve the highest reporting rates required by the IEEE Std. [1] (i.e., a new estimation every nominal period of the power system) with a three-cycle DFT-based SE algorithm, one solution would be to apply the STFT calculation expressed by (3.38) to partially overlapped portions of data. As shown in Figure 3.9, a four-stage pipeline architecture for each input channel can be adopted: based on the rising edges of a square waveform aligned to PPS and characterized by a frequency corresponding to the PMU reporting rate, each pipeline will alternately collects the required amount of data (N samples) in dedicated memories and, once they have been filled, activates a flag that triggers the SE on the previously acquired set of data.

3.3.5.2 Sliding DFT

The SDFT structure is depicted in Figure 3.10(a) and, as demonstrated in Reference 44, it can be derived from (3.18) as follows:

$$X_k(n) = \sum_{m=0}^{N-1} x(q+m) \cdot W_N^{-km} \tag{3.39}$$

$$= \sum_{m=0}^{N-1} x(q+m-1) \cdot W_N^{-k(m-1)} - x(q-1) \cdot W_N^k + x(q+N-1) \cdot W_N^{-k(N-1)} \tag{3.40}$$

$$= W_N^k \cdot \sum_{m=0}^{N-1} x(q+m-1) \cdot W_N^{-km} - x(q-1) \cdot W_N^k + x(q+N-1) \cdot W_N^{-k(N-1)} \tag{3.41}$$

$$= W_N^k \cdot (X_k(n-1) - x(q-1) + x(q+N-1)) \tag{3.42}$$

$$= W_N^k \cdot (X_k(n-1) - x(n-N) + x(n)) \tag{3.43}$$

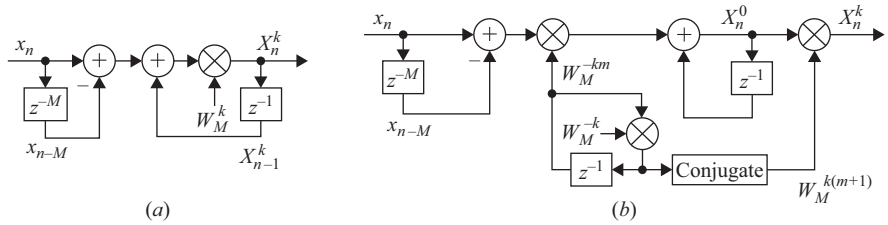

Figure 3.10 Structure of the sliding DFT (a) and of the modulated sliding DFT (b) (adapted from Reference 46)

As it can be noticed by looking at (3.43), the SDFT is a quite efficient method as, it allows to update the values of a single DFT bin every time a new sample is acquired with few multiplication and additions (see also Table 3.1).

As previously mentioned, the SDFT filter is not numerically stable and suffers from accumulated errors. Common approaches that can be found in the literature [44, 45] face this problem compromising results accuracy for guaranteed stability. This is the case of the method presented in Reference 44 where the stability is guaranteed by including in the DFT formula a damping factor r that force the SDFT pole to reside within the z-domain's unit circle (this method is here referenced as rSDFT):

$$X_k(n) = rW_N^k \cdot (X_k(n-1) - r^N x(n-N) + x(n)) \tag{3.44}$$

In this context, the next section will examine a sample-by-sample DFT update method, called MSDFT that is guaranteed stable without sacrificing accuracy [46].

3.3.5.3 Modulated sliding DFT

With reference to (3.43), it is easy to observe that the recursive formula for the computation of X_k when $k = 0$ does not involve the complex twiddle factor and is, therefore, by definition stable:

$$X_0(n) = X_0(n-1) - x(n-m) + x(n) \tag{3.45}$$

The MSDFT takes advantage of this SDFT property in order to derive a recursive formula for the DFT computation that is intrinsically stable.

In particular, by taking advantage of the so-called Fourier modulation property [6], the generic kth DFT bin can be shifted to the position $k = 0$ multiplying the input signal by the complex twiddle factor W_N^{-km}:

$$X_k(n) \Rightarrow W_N^{-km} X_0(n) = X_0(n-1) - x(n-N) \cdot W_N^{-k(m-N)} + x(n) \cdot W_N^{-km} \tag{3.46}$$

$$= X_0(n-1) + W_N^{-km} \cdot (-x(n-N) + x(n)) \tag{3.47}$$

where (3.47) is obtained thanks to the periodicity of the modulating sequence W_N^{-km}.

The twiddle factor modulation only introduces a phase shift that is changing with index m: $\angle W_N^{-km} = 0$ for $m = 0$, it increases by the W_N^{-k} factor at each iteration and

is periodically reset to 0 every N samples. Indeed, at every iteration the modulating sequence can be recursively computed as:

$$W_N^{-km} = W_N^{-k(m-1)} \cdot W_N^{-k}, \qquad m = 0, 1, \ldots, N-1 \tag{3.48}$$

It is clear that, in order to prevent that accumulated errors corrupt our estimation, the modulating sequence must be reset to 1 every N samples.[6] In view of this, the kth bin of the DFT can be derived from (3.47), as:

$$X_k(n) = W_N^{k(m+1)} \cdot X_0(n) \tag{3.49}$$

$$= W_N^{k(m+1)} \cdot (X_0(n-1) + W_N^{-km} \cdot (-x(n-N) + x(n))) \tag{3.50}$$

where $W_N^{-k(m+1)}$ compensate for the phase-shift due to the modulating sequence.

Equation (3.50) defines the MSDFT method for the update of the value of a single bin of the entire DFT spectrum and the related block scheme is given in Figure 3.10(b).

3.3.5.4 Integrating the MSDFT with signal windowing

As already discussed in Section 3.3.4.3, signal windowing is a powerful technique that allows to reduce the effects of long-range spectral leakage. Windowing is applied as in the time domain by weighting a finite sequence of samples with a particular window profile like the Hanning one (see Section 3.3.4.3):

$$x_w(n) = x(n) \cdot w(n), \quad 0 \leq n \leq N-1 \tag{3.51}$$

However, windowing by time-domain multiplication would compromise the computational simplicity of the MSDFT or any other sample-by-sample DFT calculation technique. For this reason, when adopting this kind of methods, it is of common use to apply the signal windowing in the frequency domain, namely after the DFT has been computed. Indeed, by recalling that the multiplication between two functions in the time domain corresponds to the convolution between the Fourier transform of the two functions in the frequency domain, the time-domain multiplication could be replaced by a frequency-domain convolution and obtain equivalent results.

In particular, in the case of the Hanning window, this will result into the following linear combination of adjacent DFT bins $X_k(n)$:

$$X_k(n) = -0.25 \cdot X_{k-1}(n) + 0.5 \cdot X_k(n) - 0.25 \cdot X_{k+1}(n) \tag{3.52}$$

From (3.52), it is clear that, in order to compute three windowed DFT bins, we need to compute five MSDFT bins, namely, those associated to indices $k_m + \{-2, -1, 0, 1, 2\}$.

3.4 DFT-based SE algorithms

The SE algorithm is definitely the most relevant and challenging component of a PMU. The main task of an SE algorithm is to identify and assess the parameters of the fundamental tone of a signal by using a previously acquired set of samples representing

[6]To be noticed that, for practical implementation, the modulating sequence can be either (i) precomputed and stored into memory or (ii) computed online based on (3.48).

a portion of an acquired waveform (i.e., node voltage and/or branch/nodal current). As a consequence, it mainly influences not only the PMU measurement uncertainty, but also the PMU measurement reporting latency and the maximum achievable reporting rate.

This section first reviews the literature on SE algorithms based on the DFT. This category is characterized by some inherent advantages when applied to the extraction of the main-tone parameter, namely: (i) the inherent DFT capability to isolate and identify the main tone of a discrete sinusoidal signal and (ii) reject close-by harmonics; (iii) the relatively low computational complexity, particularly when the DFT spectrum is computed through one of the well-known algorithms (e.g., FFT or sliding DFT). Nevertheless, these qualities come with non-negligible drawbacks and limitations characterizing the DFT theory that assumes a periodic signal with time-invariant parameters, at least along the observation window. The latter, on the one hand, should be as short as possible to be closer to the above-mentioned quasi-steady-state hypothesis also during power system transient; on the other hand, longer windows are needed when interested in identifying close-by tones and rejecting harmonic and inter-harmonic components. Indeed, as demonstrated in Section 3.3, the observation window T is inversely proportional to the DFT frequency resolution, as it defines both the frequency separation between consecutive DFT bins and the main lobe width.

In this respect, Section 3.4.1 presents the IpDFT, a well-established technique to estimate the parameters of a waveform out of a finite sequence of samples, which reduces the effects of spectral leakage and overcome the limitations introduced by adopting a relatively short window length. Finally, on the basis of Reference 47, Section 3.4.2 illustrates a computationally affordable method that is capable of improving the performances of standard IpDFT methods and to keep the same static and dynamic performances independently of the adopted window length.

3.4.1 The Interpolated-DFT technique

As reported in Section 3.3.3, DFT-based SE algorithms are characterized by three main sources of uncertainty: aliasing, spectral leakage and spectral sampling. Whereas the effects of aliasing can be disregarded by simply increasing the sampling frequency to values much larger than the highest spectrum component contained in the sampled signal, the combined effects of spectral leakage and spectral sampling can be detrimental if not properly treated.

As discussed in Section 3.3.3.2, spectral leakage arises when the sampling process is not synchronized with the fundamental tone of the signal under analysis and the DFT is computed over a non-integer number of cycles of the input signal [30]. Since the precise synchronization of the sampling process with the fundamental frequency component of the signal is purely theoretical (indeed such synchronization involves the a priori knowledge of the signal main tone, which is, by hypothesis, unknown), several approaches have been proposed to reduce this bias.

Among them the IpDFT technique has outperformed the others for its higher accuracies combined with a lower computational complexity. Such a method refers to the usage of:

- windowing functions aiming at mitigating the effect of long-range spectral leakage [29, 48];
- proper DFT interpolation schemes aiming at correcting the effects of the short-range leakage and reducing the inaccuracies introduced by the DFT spectral sampling (e.g., References 23, 24).

The IpDFT problem has been originally defined for a discrete sequence of samples windowed using the rectangular window [23]. In order to reduce the effects of long-range spectral leakage, the input sequence can be windowed using one of the "special" windowing functions defined in the literature (see References 29, 48). The first to combine such an approach with the IpDFT technique was Grandke in Reference 24 using the Hanning window. More recently, the IpDFT problem has been formulated using various windowing functions belonging to the Rife–Vincent class I (RVCI) [49] or parametric windowing function non-belonging to the cosine windows class, like Kaiser–Bessel or Dolph–Chebyshev windows [50].

In what follows, the IpDFT algorithm will be first formulated and solved for the case of Hanning window; then its performances are analysed, with a specific focus on the effect of the spectral interference on the accuracy of the IpDFT method.

3.4.1.1 Formulation of the IpDFT problem

The IpDFT is a technique that allows to estimate the parameters of a tone (i.e., its frequency, amplitude, and phase) by interpolating the DFT spectrum obtained from a finite sequence of N samples of a discrete signal $x(n)$ that includes the tone under analysis.

In this respect, let us consider the following finite sequence obtained by sampling with a sampling rate $F_s = 1/T_s$ a continuous waveform $x(t)$ characterized by a single frequency component at frequency f_0:

$$x(n) = A\cos\left(2\pi f_0 n T_s + \varphi\right), \quad 0 \leq n \leq N-1 \tag{3.53}$$

Let us assume to window the sequence $x(n)$ with a known windowing function $w(n)$ and compute the DFT of the obtained sequence using (3.18).

As demonstrated in Section 3.3.3.2, if the window does not contain an integer number of periods of the signal $x(n)$ leakage occurs and the main tone of the signal will be located between two consecutive DFT bins (see Figure 3.11). Its frequency can therefore be expressed as follows:

$$f_0 = (k_m + \delta)\Delta f \tag{3.54}$$

being k_m the index of the DFT bin characterized by the highest amplitude and $-0.5 \leq \delta < 0.5$ a fractional correction term.

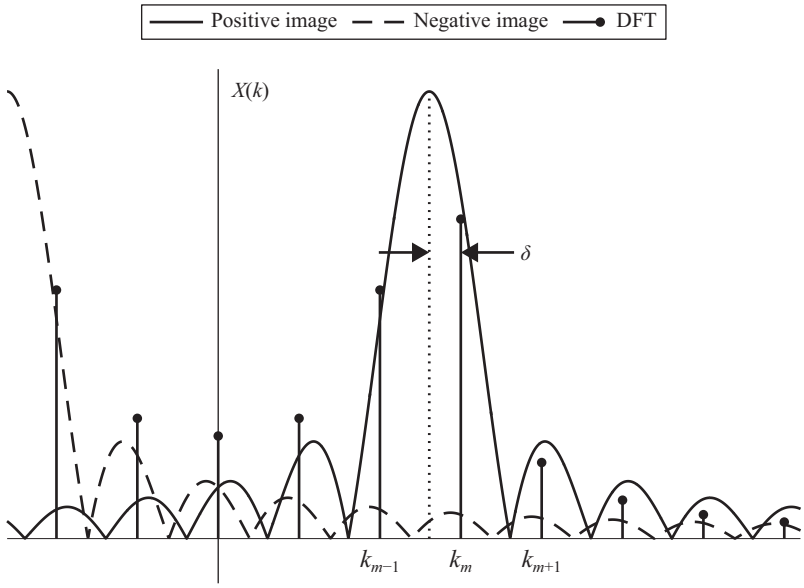

Figure 3.11 Zoom on the portion of the DFT spectrum surrounding the bin $X(k_m)$ that highlights the correction term δ and the spectral contributions produced by the positive (continuous line) and negative (dashed line) images of the spectrum

From (3.54), the IpDFT problem can be formulated as follows:

Based on the DFT spectrum $X(k)$ of the signal $x(n)$ analysed with the known windowing function $w(n)$, find the correction term δ that better approximates the exact location of the main spectrum tone.

According to the adopted window profile and number of DFT bins used to perform the interpolation, various analytical or approximated solutions to the problem can be given [49]. In what follows, the solution will be presented for a signal windowed using a Hanning window (see (3.55)–(3.57)) and using a two-point interpolation.

3.4.1.2 Solution of the IpDFT problem using the Hanning window

The Hanning window (also known as Hann window) is defined as:

$$w_H(n) = \frac{1 - \cos\left(\frac{2\pi n}{N}\right)}{2}, \quad n \in [0, N-1] \tag{3.55}$$

and its Fourier transform is

$$W_H(\omega) = -0.25 \cdot D_N\left(\omega - \frac{2\pi}{N}\right) + 0.5 \cdot D_N(\omega) - 0.25 \cdot D_N\left(\omega + \frac{2\pi}{N}\right) \tag{3.56}$$

being $D_N(\omega)$ the *Dirichlet kernel* defined as:

$$D_N(\omega) = e^{-j\omega(N-1)/2}\frac{\sin\left(\frac{\omega N}{2}\right)}{\sin\left(\frac{\omega}{2}\right)} \tag{3.57}$$

also known as the generalized Fourier transform of the rectangular window.

As demonstrated in Section 3.3, the spectrum of the sampled signal $x(n)$ in (3.53) can be expressed in terms of its positive and negative images:

$$X(f) = X^+(f) + X^-(f) \tag{3.58}$$

$$= \frac{A}{2}e^{j\psi}W_H(f - f_0) + \frac{A}{2}e^{-j\psi}W_H(f + f_0) \tag{3.59}$$

being $W_H(f)$ the Fourier transform of the Hanning window, A and ψ the amplitude and instantaneous phase of the signal $x(t)$, respectively.

Assuming that the effects of leakage are properly compensated by windowing, we can reasonably neglect the long-range spectral leakage produced by the negative spectrum image on the positive frequency range and assume that the DFT bins in the positive frequency range are only generated from the positive image of the spectrum, namely:

$$X(k) \approx X^+(k), \quad 0 \le k \le \frac{N}{2} \tag{3.60}$$

The fractional term δ can be estimated starting from the ratio between the two highest bins of the DFT $X(k_m)$ and $X(k_m + \varepsilon)$ that, for $N \gg 0$, can be approximated as follows [49]:

$$\frac{X(k_m + \varepsilon)}{X(k_m)} \approx \frac{W_H\left((\varepsilon - \delta)\cdot\frac{2\pi}{N}\right)}{W_H\left(-\delta\cdot\frac{2\pi}{N}\right)} \tag{3.61}$$

where $W_H(\cdot)$ is the Fourier transform of the Hanning window (see (3.56)) and

$$\varepsilon = \begin{cases} 1 & \text{if } |X(k_m + 1)| > |X(k_m - 1)| \\ -1 & \text{if } |X(k_m + 1)| < |X(k_m - 1)| \end{cases} \tag{3.62}$$

If $N \gg 0$, the following approximation holds:

$$e^{\pm j\pi(N-1/N)} \approx -1 \pm \frac{j\pi}{N} \tag{3.63}$$

and the absolute value of $W_H(\omega)$ can be approximated as:

$$|W_H(\omega)| \approx \left|\sin\left(\frac{\omega N}{2}\right)\right| \cdot \left|-\frac{0.25}{\sin\left(\frac{\omega}{2} - \frac{\pi}{N}\right)} + \frac{0.5}{\sin\left(\frac{\omega}{2}\right)} - \frac{0.25}{\sin\left(\frac{\omega}{2} + \frac{\pi}{N}\right)}\right| \tag{3.64}$$

By replacing (3.64) in (3.61) and recalling that $\lim_{x\to 0} \sin(x) = x$, we get:

$$\begin{aligned}\frac{X(k_m+\varepsilon)}{X(k_m)} &= \frac{\left|W_H\left((\varepsilon-\delta)\cdot\frac{2\pi}{N}\right)\right|}{\left|W_H\left(-\delta\cdot\frac{2\pi}{N}\right)\right|} \\ &\approx \left|\frac{0.25}{\delta-\varepsilon+1}-\frac{0.5}{\delta-\varepsilon}+\frac{0.25}{\delta-\varepsilon-1}\right| \Big/ \left|\frac{0.25}{\delta+1}-\frac{0.5}{\delta}+\frac{0.25}{\delta-1}\right| \\ &= \left|\frac{0.5}{\delta(\delta-\varepsilon)(\delta-2\varepsilon)}\right| \left|\frac{\delta(\delta+1)(\delta-1)}{-0.5}\right| \\ &= \left|\frac{\delta+\varepsilon}{\delta-2\varepsilon}\right| \end{aligned} \tag{3.65}$$

that, solved for the frequency correction δ gives:

$$\widehat{\delta} = \varepsilon\,\frac{2\,|X(k_m+\varepsilon)| - |X(k_m)|}{|X(k_m)| + |X(k_m+\varepsilon)|} \tag{3.66}$$

where the $\widehat{\ }$ symbol was used to indicate the estimation of the fractional correction term δ. The waveforms parameters (i.e., its frequency, amplitude and phase) can then be computed as follows:

$$\widehat{f} = (k_m+\widehat{\delta})\Delta f \tag{3.67}$$

$$\widehat{A} = |X(k_m)|\left|\frac{\pi\widehat{\delta}}{\sin(\pi\widehat{\delta})}\right|\left|\widehat{\delta}^{\,2}-1\right| \tag{3.68}$$

$$\widehat{\varphi} = \angle X(k_m) - \pi\widehat{\delta} \tag{3.69}$$

3.4.1.3 Optimal selection of the IpDFT parameters for SE

The relevant parameters of the IpDFT technique should be properly chosen according to the characteristics of the input sequence $x(n)$ (i.e., the DFT spectrum $X(k)$).

In this respect, this section presents the optimal selection of the three main IpDFT parameters (i.e., the *sampling rate*, the *window length*, and the *window profile*) when applying such a technique to SE and argument their choice by making reference to the signal model presented in Section 3.2.1 (see (3.2)). In particular, in the following of this chapter, both the SE algorithm formulation and the discussion of the experimental results will make reference to a DFT calculated on a sequence of samples obtained by sampling the input signal $x(t)$ with a sampling rate F_s of 50 kHz over a window length T containing three periods of a waveform at the nominal frequency of a power system f_0 and windowed using a Hanning window.

Sampling rate

The IpDFT sampling rate F_s must be primarily selected following the considerations presented in Section 3.3.4.1 regarding the detrimental effects of aliasing. In this respect, it is worth pointing out that in the field of power system, harmonic and inter-harmonic components rarely exceed few kilohertz and consequently a PMU that does not adopt any anti-aliasing filter must sample the signal with a sampling rate F_s of

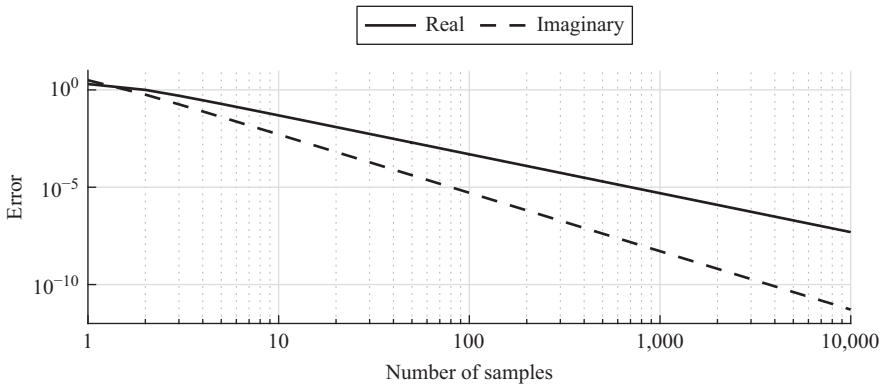

Figure 3.12 Behaviour of the real (continuous line) and imaginary parts (dashed line) of $e^{\pm j\pi(N-1/N)} - (-1 \pm j\pi/N)$ *(see* (3.63)*) as a function of the number of samples N*

at least 10 kHz. Additionally, a relatively high sampling rate allows to process a higher number of samples and consequently mitigate the effects of wideband noise.

Last but not least, it should not be forgotten that, the sampling rate F_s together with the window length T, defines the number of samples N to be processed by DFT. In this respect, it is worth pointing out that the IpDFT solution given in (3.66) for the case of the Hanning window (the same hypothesis is actually valid for any IpDFT estimator based on the class of RVCI windows) can only be obtained if the number of samples N is sufficiently large so that the approximation presented in (3.63) is valid. Figure 3.12 shows the residuals of (3.63). As it can be seen, by adopting a relatively high sampling rate F_s, the number of samples N can be increased up to values where the effects of such an approximation are not visible and it can be considered exact.

Window length

As reported in Section 3.3.4.2, the window length T is the most critical DFT parameter, and it must be selected first of all to guarantee the stationarity of the sequence of samples $x(n)$. Additionally, as reported in Section 3.5.1.3, window lengths directly affect the PMU RTs and measurement reporting latencies. In this respect, a shorter window length including, at most, four periods of a signal at the nominal frequency of the power system f_0, more easily ensures the stationarity hypothesis in most of the PMU operating conditions. At the same time, it guarantees to satisfy the most stringent PMU RT and measurement reporting latency requirements dictated by Reference 1, particularly with respect to the P-class measurement requirements (see also Section 3.5.1.2).

Nevertheless, this choice comes with at the price of a reduced DFT frequency resolution that, depending on the adopted window profile, might not allow to detect nearby tones like inter- or sub-harmonics. Furthermore, as it will be discussed in the next section, shorter window lengths amplify the effect of long-range spectral leakage and therefore the spectral interference between close-by tones.

Window profile

The solution of the IpDFT problem (Section 3.4.1.2) has been presented when using a Hanning window in order to reduce the effects of long-range spectral leakage. This windowing function has demonstrated to represent a good trade-off between the long-range spectral leakage suppression (i.e., the side-lobe levels) and the DFT frequency resolution (i.e., the main lobe width). In particular, compared to the rectangular window, the Hanning window is characterized by a wider (almost double) main lobe but a much higher side-lobes decaying rate (see Figure 3.8).

Nevertheless, a similar solution could be analytically derived for any other function belonging to the category of RVCI windows or based on a polynomial approximation for the class of parametric non-cosine windows (see Reference 49 for the IpDFT solution for both category of windows).

In general, the window profile must be chosen according to the field of application of the IpDFT technique. Whether the interest is reducing the effect of long-range spectral leakage produced by interfering tones or it is identifying and estimating the parameters of nearby frequency components, a window profile characterized by lower side lobes or a narrower main lobe must be preferred, respectively.

3.4.1.4 IpDFT sensitivity to spectral interference

The IpDFT is a powerful method to artificially increase the DFT frequency resolution, and accurately estimate the parameters of a sinusoidal waveform. Nevertheless, its accuracy is mainly limited by the *spectral interference* produced by nearby tones that might not allow to distinguish the portion of spectrum that has been generated by the tone under analysis from other frequency components.

Indeed, as reported in Sections 3.4.1.1 and 3.4.1.2, the main hypothesis behind the analytical solution of the IpDFT problem is that the DFT bins used to perform the interpolation are only generated by the tone under analysis. As a consequence, the IpDFT theory assumes that, independently of the adopted window profile, the DFT spectrum only contains a single component characterized by a frequency $f_0 \gg \Delta f$, so that the positive and negative images of the spectrum are sufficiently distant and the approximation expressed by (3.60) is satisfied. In case the input signal includes more frequency components (e.g., harmonics and/or inter- and sub-harmonics), they should be sufficiently separate so that the effects of long-range spectral leakage can be neglected. If these assumptions are not satisfied, the DFT bins used to perform the interpolation, and therefore the IpDFT estimations, might be partially biased by the tails of the nearby tones. Eventually, if the energy content of the spectral interference exceed the one of the tone under analysis, the tone detectability is not even guaranteed.

As reported in the previous section, the application of the IpDFT technique to the field of SE requires the adoption of quite short windows, which contain few periods of the signal under analysis, in order to assume the stationarity of the signal and, at the same time, reduce the PMU RTs and measurement reporting latencies. This choice causes the energy of the DFT spectrum to be concentrated in the lower frequency range and the positive and negative images of the spectrum to be relatively close. Independently of the adopted window profile, the side lobes of the negative image of the spectrum leak in the positive frequency range and bias the DFT bins used to

perform the interpolation that are not only originated by the positive image of $X(k)$ but also influenced by the tails produced by the negative image of the spectrum (see Figure 3.11). The assumption expressed by (3.60) cannot be satisfied and the IpDFT estimations are consequently degraded.

This phenomenon can be slightly reduced by adopting windowing functions with good side-lobe behaviours [48], but most of the time, this is not sufficient to achieve the higher accuracies required by certain synchrophasor-based applications. In this respect, the following of this chapter will focus on the formulation of an SE algorithm that enhances the IpDFT performances by combining such a technique with an iterative approach for the compensation of the spectral interference produced by the negative image of the main tone of the spectrum.

3.4.2 The iterative-Interpolated DFT technique

The performances of any IpDFT method are definitely related to the accuracy in the estimation of the fractional term δ that, ideally, could be improved by processing a DFT spectrum that only contains the positive image of the tone under analysis. In this respect, in what follows, an iterative technique for the compensation of the spectral interference produced by the negative image of the main tone of the spectrum is proposed and combined with the two-point IpDFT estimator presented in Section 3.4.1.2, to derive a novel SE algorithm that hereafter will be called i-IpDFT.

3.4.2.1 Iterative compensation of the spectral interference

By neglecting the spectral interference produced by other tones, the DFT spectrum of the signal $x(n)$ in (3.53) can be expressed, as shown in (3.58), in function of the contribution of the positive and negative images of the main tone. As a consequence, the highest and second-highest DFT bins, which are used to estimate δ according to (3.66), can be expressed as:

$$X(k_m) = \frac{1}{B}\left[\frac{A}{2}e^{j\psi}\cdot W(-\delta) + \frac{A}{2}e^{-j\psi}\cdot W(2k_m+\delta)\right] \tag{3.70}$$

$$X(k_m+\varepsilon) = \frac{1}{B}\left[\frac{A}{2}e^{j\psi}\cdot W(\varepsilon-\delta) + \frac{A}{2}e^{-j\psi}\cdot W(2k_m+\varepsilon+\delta)\right] \tag{3.71}$$

where $W(\cdot)$ is the Fourier transform of the adopted windowing function and the spectral interference coming from the negative spectrum image is represented by the following terms:

$$X^{-}(k_m) \triangleq \frac{1}{B}\left[\frac{A}{2}e^{-j\psi}\cdot W(2k_m+\delta)\right] \tag{3.72}$$

$$X^{-}(k_m+\varepsilon) \triangleq \frac{1}{B}\left[\frac{A}{2}e^{-j\psi}\cdot W(2k_m+\varepsilon+\delta)\right] \tag{3.73}$$

Since $W(\cdot)$ is analytically known once the windowing function has been selected, the amount of spectral interference generated by the negative image of the spectrum on the above DFT bins can be estimated. In particular, (3.72) and (3.73) can be evaluated using an initial estimation of the waveform parameters $\widehat{A}$ and $\widehat{\psi}$ obtained

using the classical IpDFT technique presented in Section 3.4.1.2. These estimations can then be subtracted from the DFT bins to reduce the spectral interference so that the "compensated" DFT bins

$$\widehat{X}(k_m) = X(k_m) - X^{-}(k_m) \tag{3.74}$$

$$\widehat{X}(k_m + \varepsilon) = X(k_m + \varepsilon) - X^{-}(k_m + \varepsilon) \tag{3.75}$$

are mostly generated by the positive image of the spectrum.

Then, the estimation of the fractional term δ and the related waveform parameters can be improved by re-using the IpDFT algorithm on the new set of DFT bins. This process can be either iterated a predefined number of times or performed until a given convergence criterion is achieved and bring to a more accurate estimation of the set of parameters $\{\widehat{f}, \widehat{A}, \widehat{\psi}\}$.

3.4.2.2 Formulation of the i-IpDFT method

The proposed i-IpDFT SE algorithm is presented, on the basis of Reference 47, in form of a pseudo-code (see next page) that explains the fundamental steps necessary to correctly estimate the synchrophasor according to the i-IpDFT technique.

First, the continuous input waveform (voltage or current) is sampled with a sampling rate F_s that is sufficiently high to neglect the effects of aliasing on the DFT spectrum. In this respect, in Section 3.4.1.3, we have adopted a sampling rate F_s of 50 kHz. The samples are then collected into a finite sequence of length N that should be sufficiently short so that the signal can be assumed stationary at least within its boundaries. In this respect, a window containing three periods of a signal at the nominal frequency f_0 (namely, $T = NT_s = 3/f_0$) has proven to be a good trade-off between the accuracy and RT requirements (see Section 3.4.1.3). The finite sequence of samples is then windowed using a Hanning window and the three highest bins of the DFT, namely those corresponding to DFT indices $k = k_m + \{-1, 0, +1\}$, computed according to what stated in (3.18).[7]

Next, a first estimation of the parameters of the main tone can be given according to the classical two-point IpDFT technique based on a Hanning window formulated in Section 3.4.1.2. Although such an estimation could be considerably affected by the effect of the spectral interference produced by the image component, it can be used to approximate the effects of its "tails" on the two highest DFT bins that are used to estimate δ according to what stated in Section 3.4.2.1. Such an amount can be subtracted from the original DFT spectrum to reduce the effect of spectral interference and the waveform parameters estimation refined. As shown in the pseudo-code, this approach is either iterated a predefined amount of time or until the spectral interference compensation does not bring any additional advantage.

As it can be noticed, the i-IpDFT technique has a clear advantage with respect to other SE methods: the algorithm is composed by few well-defined macro-functionalities that are often recalled along the execution of the pseudo-code through

[7]It is worth pointing out that by adopting a sufficiently short window length T, the index corresponding to the DFT maximum k_m can be fixed a priori and calculated as $k_m = \lceil f_0/\Delta f \rfloor = \lceil f_0 N/F_s \rfloor$. Consequently, there is no need to perform a maximum search on the DFT bins.

a for loop structure. The i-IpDFT SE algorithm can therefore exploit the speed of high-speed digital architectures like field programmable gate arrays (FPGAs) and reduce the required amount of hardware resources simply reusing already allocated portion of the hardware design.

3.5 Performance analysis of SE algorithm

This section first presents a procedure to assess the performances of SE algorithms that is based on the IEEE Std. C37.118. Next, it verifies the performances of the i-IpDFT SE algorithms by making reference to the most relevant tests defined in Reference 1.

The reader should consider that this section is only meant to quantify the performances of the adopted SE algorithm and does not deal with the other components of a PMU that might introduce a further and non-negligible uncertainty to the estimated synchrophasor (see Section 3.2.5).

3.5.1 The IEEE Std. C37.118

The performances of PMUs are constrained by a single international standard, the IEEE Std. C37.118. This standard derives from a preliminary version of an IEEE Standard for synchrophasors, the IEEE Std. 1344-1995 [34], and has been first issued in 2005 [51], reviewed in 2011 [1, 35], and amended in 2014 [52]. It is composed

Algorithm 1 The iterative-IpDFT synchrophasor estimation algorithm.

procedure ITERATIVE-INTERPOLATED DFT($x(t)$) ▷ $x(t)$ is the input signal
  Signal sampling: $x(n) = x(nT_s)$ ▷ Sampling rate: $F_s = 1/T_s = 50$ kHz
  Signal buffering: $x(n), \quad n = 0, \ldots, N-1$ ▷ Window length $T = NT_s = 3/f_0$
  Signal windowing (Hanning): $x_h(n) = x(n) \cdot w_H(n)$ ▷ see (3.55);
  DFT calculation: $X(k), \quad k = k_m + \{-1, 0, +1\}$ ▷ see (3.18);
  Two-point DFT interpolation: $\left\{\widehat{f}, \widehat{A}, \widehat{\psi}\right\}_0$ ▷ see (3.67)–(3.69);
  for $r = 1 \rightarrow R$ **do**
    Spectral interference estimation: $X^{-}(k)$ ▷ see (3.72) and (3.73) ;
    DFT enhancement: $\widehat{X}(k)$ ▷ see (3.74) and (3.75);
    Two-point DFT interpolation: $\left\{\widehat{f}, \widehat{A}, \widehat{\psi}\right\}_r$ ▷ see (3.67)–(3.69);
    if $\left\{\widehat{f}, \widehat{A}, \widehat{\psi}\right\}_r \approx \left\{\widehat{f}, \widehat{A}, \widehat{\psi}\right\}_{r-1}$ **then**
      break for
    end if
  end for
  return $\left\{\widehat{f}, \widehat{A}, \widehat{\psi}\right\}_r$
end procedure

by two parts: (i) Part I, the *IEEE Std. for Synchrophasor Measurements for Power Systems*, deals with the synchrophasor terminology and the synchrophasor measurement requirements and compliance verification; (ii) Part II, the *IEEE Standard for Synchrophasor Data Transfer for Power Systems*, mainly defines the synchrophasor message format, message types, and communications.

The PMU compliance to the IEEE Std. is achieved by satisfying both the measurement requirements specified in Reference 1 and amended in Reference 52 and the communication requirements as described in Reference 35. Whereas the latter are straightforward to be accomplished, the former is a more challenging achievement as it involves several engineering competencies necessary to build a compliant PMU prototype. To this purpose, Reference 1 has proposed a metrological procedure aimed at assessing the PMU accuracies during both steady state and dynamic conditions of a power system. This is done by defining specific tests and reference signals, aimed at artificially simulating various operating conditions of the electrical grid, together with the related compliance requirements. The PMU compliance is then assessed by comparing the PMU performances to the IEEE Std. requirements and verifying if they respect the previously defined limits.

In what follows, the PMU compliance verification procedure proposed in Reference 1 is summarized and commented. For further details, the reader should make reference to what originally stated in the IEEE Standard [1], the related IEEE Guide [38] and the latest Test Suite Specification (TSS) [53].

3.5.1.1 Reporting rates and reporting times

Synchrophasor measurements produced by PMUs must be reported regularly at a reporting rate F_r that is an integer number of frames per second [1]. The reporting times shall be evenly spaced through each second, with the time of the first frame within the second coincident with the UTC-second rollover (i.e., with a fractional second of 0).

According to Reference 1, a PMU shall support the reporting rates 10, 25, 50 or 10,12, 15, 20, 30, 60 frames-per-second (fps) depending on whether the power system frequency f_0 is 50 or 60 Hz, respectively. Higher reporting rates, such as 100 or 120 fps, are also encouraged in the Standard to support time-critical applications like power system protection and fault management [54]. Nevertheless, it is worth pointing out that only those PMU characterized by a shorter window length can afford to push their reporting rates up to these values, as the correlation between consecutive measurements can make such an increased information rate useless.

3.5.1.2 Performance classes

PMUs shall be tested against the expected *operating conditions* and the targeted *power system applications*. With respect to the latter, the IEEE Std. [1] has defined two performance classes, corresponding to two distinct PMU applications and different compliance requirements:

- *P-class* is intended for Protection applications or any application requiring fast RTs and reduced reporting latencies (see Section 3.5.1.3).

- *M-class* is intended for Measurement applications where more importance is given to the accuracy of the PMU estimations, and particularly to its capability to reject inter-harmonics, rather than their RTs and reporting latencies.

It is worth noting that the performance classes defined in the IEEE Std. [1] do not discriminate between the use of PMUs in transmission or distribution networks and the various test types and compliance requirements have been derived by assuming the operating conditions of transmission networks. This is because PMUs have been originally deployed at such a level, mainly for the higher investment costs and the critical reliability of this infrastructure. As a consequence, it is important to keep in mind that such a compliance verification might not be sufficient for a PMU that wants to operate at the power distribution level.

3.5.1.3 PMU performance evaluation

The evaluation of the PMU performances is typically performed by a dedicated PMU calibrator capable of characterizing the metrological performances of the PMU under test by comparing its estimations to a "true" value[8] and assessing its conformity to some predefined accuracy limits.

In what follows, in the following sections, the metrics defined in Reference 1 to evaluate the PMU estimation errors together with those for the PMU RT and measurement reporting latency are presented.

Total vector error

The PMU accuracy in estimating the true synchrophasor can be expressed independently in terms of the amplitude and phase errors or the real- and imaginary-part errors if rectangular coordinates are adopted. This is, for instance, the approach used in the case of instrument transformers, where the acceptable errors are expressed separately in terms of the allowed phase angle and magnitude error (see Reference 55).

Nevertheless, sometimes it is useful to express the SE error with a single value that includes both components. This quantity has been defined in Reference 1 and is called *total vector error* (TVE). The TVE is a real number that expresses the Euclidean distance between the true and estimated synchrophasors, normalized with respect to the amplitude of the true synchrophasor (see Figure 3.13):

$$TVE \triangleq \frac{\left|\widehat{X} - X\right|}{|X|} \tag{3.76}$$

$$= \frac{\left|\left(\widehat{X}_r + j\widehat{X}_i\right) - (X_r + jX_i)\right|}{|X_r + jX_i|} \tag{3.77}$$

$$= \sqrt{\frac{\left(\widehat{X}_r - X_r\right)^2 + \left(\widehat{X}_i - X_i\right)^2}{X_r^2 + X_i^2}} \tag{3.78}$$

[8] Since the "true" value of a quantity is hidden by definition, in what follows, the term "true" will be used to define a reference quantity characterized by a variance that is known and can be a priori considered much smaller than the one of the PMU estimation.

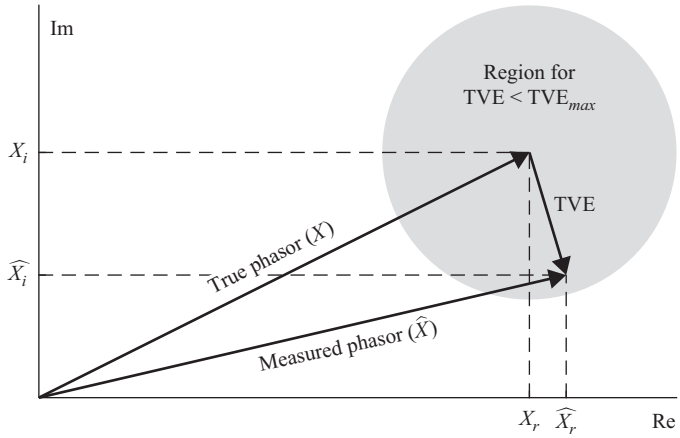

Figure 3.13 Complex plane plot showing the "true" phasor and the measured one that is, in this case, compliant with the TVE requirements (grey area centered around the "true" phasor) (adapted from Reference 1)

where $\widehat{X}$ identifies the synchrophasor estimated by the PMU, X the true one, and the subscripts r and i identify the real and imaginary parts of the synchrophasor, respectively.

The TVE can be used to set the PMU accuracy requirements by defining the maximum allowable limit like any other error quantity. It can be visualized as a circle centred around the true synchrophasor X characterized by a radius corresponding to the maximum allowable TVE (that also correspond to the maximum allowable magnitude error). If the estimated synchrophasor falls within the circle, the PMU is compliant else it is not (see Figure 3.13).

Treating a single number to characterize the PMU accuracy in estimating the synchrophasor has its advantages and disadvantages. Among these, the impossibility to decouple the contribution of amplitude and phase estimation error to understand eventual PMU asymmetries in the SE. For these reasons, in what follows, the TVE will be considered together with the amplitude and phase errors as additional metrics.

Frequency error

The frequency error (FE) is defined in the IEEE Std. C37.118 [1] as follows:

$$FE \triangleq \left| f - \widehat{f} \right| \tag{3.79}$$

being f the true frequency value and $\widehat{f}$ the one estimated by the PMU.

ROCOF error
The rate of change of frequency error (RFE) is defined in the IEEE Std. C37.118 [1] as follows:

$$RFE \triangleq \left| ROCOF - \widehat{ROCOF} \right| \tag{3.80}$$

being $ROCOF$ the true ROCOF value and $\widehat{ROCOF}$ the one estimated by the PMU.

Magnitude error
The magnitude error is defined as follows:

$$\varepsilon_A \triangleq A - \widehat{A} \tag{3.81}$$

being A the true magnitude of the signal and $\widehat{A}$ the one estimated by the PMU.

Phase error
The phase error is defined as follows:

$$\varepsilon_\psi \triangleq \psi - \widehat{\psi} \tag{3.82}$$

being ψ the true instantaneous phase of the signal and $\widehat{\psi}$ the one estimated by the PMU.

Response time
The RT is defined as the transition time between two consecutive steady-state measurements, before and after a step change is applied at one or more waveforms acquired by the PMU.

It is evaluated by applying a step change in the amplitude or phase of the input waveforms and measuring the time interval where the PMU errors exceed some predefined accuracy limits (see Figure 3.14). If t_{start} is the time of the first PMU estimation that exceed the limit and t_{end} is the time of the first PMU estimation that re-enters and stays within that limit, then the RT can be computed as:

$$RT \triangleq t_{end} - t_{start} \tag{3.83}$$

The evaluation of the RT is useful to understand the effect of the adopted window length during power system transients.

Delay time
The delay time is defined as the time interval between the instant that a step change is applied to the input of a PMU and measurement time that the stepped parameter achieves a value that is halfway between the initial and final steady-state values [1].

It is evaluated by applying a step change in the amplitude or phase of the input waveforms and measuring the time interval between the effective time the step change takes place and the moment the PMU estimation of the stepped parameter reached a value that is halfway between the initial and final steady-state values (see Figure 3.14).

The evaluation of the delay time is useful to verify that the timestamp has been properly compensated for any delay introduced by the PMU filtering system.

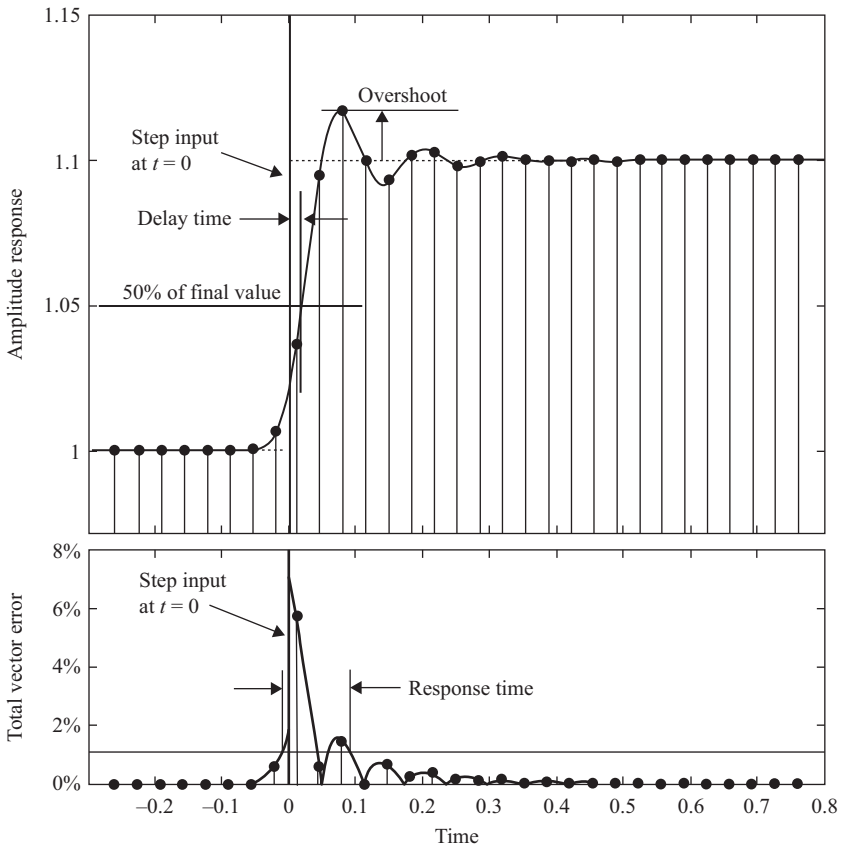

Figure 3.14 Representation of the PMU RT, delay time and maximum overshoot during an amplitude step change with a TVE limit of 1% (adapted from Reference 1)

Maximum overshoot

The maximum overshoot is defined as the measure of the maximum peak value of the estimated synchrophasor by the PMU during a step change of the instantaneous amplitude or phase (see Figure 3.14).

Reporting latency

The reporting latency is the time delay between the time a specific event has occurred in the power system and the time it is measured and reported by the PMU. The main contribution to this quantity are: (i) the adopted window length, (ii) the processing time needed by the SE algorithm and (iii) the processing time needed by the encapsulation and streaming process.

It is typically measured by connecting the PMU point-to-point with a PMU calibrator that has the possibility to time-tag the moment a PMU data frame is received at

Table 3.2 IEEE Std. C37.118 compliance requirements for steady-state conditions (in the table F_s is the PMU reporting rate). The symbol "–" means that either the specific performance class does not include that specific test or the specific requirements have been suspended by the IEEE Std. C37.118 amendment [52]

Influence quantity		TVE (%)		FE (Hz)		RFE (Hz/s)	
		P-class	M-class	P-class	M-class	P-class	M-class
Signal frequency		1	1	0.005	0.005	0.4	0.1
Signal magnitude		1	1	0.005	0.005	0.4	0.1
Harmonic distortion	$F_r > 20$	1	1	0.005	0.025	0.4	–
	$F_r \leq 20$	1	1	0.005	0.005	0.4	–
OOB interference		–	1.3	–	0.01	–	–

its network adapter. By assuming the network delays negligible, the reporting latency can be computed as follows:

$$RL \triangleq t_r - t_s \tag{3.84}$$

being t_s the PMU timestamp of a specific data frame and t_r the time that data frame has been received in the calibrator.

The maximum allowable reporting latencies are independent of the testing conditions and equal to $2/F_r$ and $7/F_r$ for P-class and M-class, respectively, being F_r the PMU reporting rate.

3.5.1.4 The steady-state compliance tests

Steady-state conditions are defined as conditions where the instantaneous parameters of the reference signals (including also the parameters of the interfering signals other than the main tone) are constant along the whole duration of each sub-test. According to Reference 1, the PMU steady-state compliance can be accomplished by satisfying the accuracy requirements for TVE, FE and RFE of the specific performance class, while varying the influence quantities that are listed below. Table 3.2 summarize the IEEE Std. C37.118 [1] steady-state compliance limits (including the latest amendment reported in Reference 52) for TVE, FE and RFE for both performance classes P and M.

Signal frequency

During this test, the reference signals are composed by a single sinusoidal component characterized by a frequency f that is varied by 0.1 Hz between each sub-test, whereas the other tone parameters (A and φ) are kept constant. The frequency bandwidth to be tested depends on the targeted performance class and reporting rate but cannot be higher than 10 Hz, centred around the nominal frequency f_0 (e.g., in the case of a

nominal frequency of 50 Hz, the widest frequency range to be tested is between 45 and 55 Hz).

Signal magnitude (voltage and current)
During this test, the reference signal is composed by a single sinusoidal component characterized by an amplitude A that is varied by 10% between each sub-test, whereas the other tone parameters (f and φ) are kept constant. The amplitude range to be tested depends on the targeted performance class and whether the measured quantity is a voltage or a current. In general, it cannot be lower than 10% of the nominal amplitude A_0 and higher than 120% of A_0 for voltage signals or 200% of A_0 for current signals.

Harmonic distortion
This test allows to assess the influence of harmonics on the quality of the estimated synchrophasor, frequency, and ROCOF. It assumes that a steady-state single-tone signal at the nominal frequency f_0 and characterized by a nominal amplitude A_0 is corrupted by a single superposed harmonic characterized by an amplitude that is either 1% or 10% of the nominal amplitude A_0 in case of P-class or M-class compliance, respectively. The harmonic order is varied between each test, starting from the second up to the 50th harmonic.

Out-of-band interference
This test allows to assess the influence of inter- and sub-harmonics on the quality of the estimated synchrophasor, frequency, and ROCOF and it is only defined for M-class compliance. Out-of-band (OOB) compliance must be tested with a main-tone signal characterized by a frequency within $f_0 - 0.1F_r/2$ and $f_0 + 0.1F_r/2$, being F_r the reporting rate and $F_r/2$ the associated Nyquist limit (e.g., between 47.5 and 52.5 Hz if f_0 is 50 Hz) and a nominal amplitude A_0. Single inter- or sub-harmonic signals must be superposed to such a main tone and be characterized by an amplitude equal to 10% of A_0 and a frequency that is either within 10 Hz and $f_0 - F_r/2$ or within $f_0 + F_r/2$ and $2f_0$.

3.5.1.5 The dynamic compliance tests

Dynamic conditions are defined in Reference 1 as conditions where the instantaneous parameters of the main tone of the reference signal (namely its frequency f, amplitude A, and initial phase φ) are not constant along the duration of each sub-test. Therefore, with the term dynamic conditions, the IEEE Std. [1] does not include the evaluation of the PMU performances during dynamic behaviour of any interfering signals. According to Reference 1, the PMU dynamic compliance can be accomplished by satisfying the accuracy requirements for TVE, FE and RFE together those for the RT for the specific performance class, during the following tests.

Measurement bandwidth
This test aims at testing the quality of the PMU estimations during increasing variation of the instantaneous amplitude $A(t)$ and phase $\psi(t)$ of the main tone of the reference signal. In particular, during this test, the reference signals are characterized

by independent sinusoidal amplitude or phase modulations according to the following formula:

$$x(t) = A_0 \left[1 + k_a \cos\left(2\pi f_m t\right)\right] \cdot \cos\left[2\pi f_0 t + k_p \cos\left(2\pi f_m t - \pi\right)\right] \tag{3.85}$$

being f_m the modulating frequency, k_a and k_p the amplitude and modulation factors, respectively. According to Reference 1, f_m must be varied by steps of 0.2 Hz or smaller between each sub-test, within a range that goes from 0.1 to $F_m \triangleq \min\left(F_r/10, 2\right)$ or from 0.1 to $F_m \triangleq \min\left(F_r/10, 5\right)$ in the case of P-class or M-class compliance, respectively. On the other hand, the modulation factors k_a and k_p are set constant to 0.1 and the two modulations applied separately.

System frequency ramp

This test is defined to verify the correct positioning of the timestamp within the time window and to test the linearity of the PMU "filter". During this test, the main-tone parameters are kept constant except the instantaneous frequency that is varied linearly with a constant rate of 1 Hz/s. Both positive and negative ramps must be tested within a frequency range that is between $f_0 - 2\,\text{Hz}$ and $f_0 + 2\,\text{Hz}$ for P-class compliance and between $f_0 - \min\left(F_r/5, 5\right)$ Hz and $f_0 + \min\left(F_r/5, 5\right)$ Hz in the case of M-class compliance.

Step changes in amplitude and phase

This test is designed to simulate sudden power system events like voltage and current variations during faults, short circuits, or the synchronization of islanded/separated networks. It is aimed at testing the PMU RT, that is mainly influenced by the adopted time-window length. According to Reference 1, the step change is applied simultaneously to all three phases and to both voltage and current inputs. The IEEE Std. requires to test 10% positive and negative amplitude steps and 10° positive and negative phase steps.

Tables 3.4 and 3.5 summarize the IEEE Std. C37.118 [1] dynamic compliance limits (including the latest amendment reported in Reference 52) for TVE, FE and RFE (see Table 3.3) together with those for the RT (see Table 3.4), delay time and maximum overshoot (see Table 3.5) for both performance classes P and M.

Table 3.3 IEEE Std. C37.118 limits for TVE, FE and RFE during dynamic conditions (in the table F_m is the maximum modulating frequency for a specific PMU reporting rate F_r)

Test	**TVE (%)**		**FE (Hz)**		**RFE (Hz/s)**	
	P-class	**M-class**	**P-class**	**M-class**	**P-class**	**M-class**
Measurement bandwidth	3	3	$0.03F_m$	$0.06F_m$	$0.18\pi F_m^2$	$0.18\pi F_m^2$
Frequency ramp	1	1	0.01	0.01	0.4	0.2
Amplitude/phase steps	1	1	0.005	0.005	0.4	0.1

Table 3.4 IEEE Std. C37.118 limits for RT during amplitude and phase steps

Test	Phasor RT (s)		Frequency RT (s)		ROCOF RT (s)	
	P-class	**M-class**	**P-class**	**M-class**	**P-class**	**M-class**
Amplitude/ phase steps	$2/f_0$	$7/F_r$	$4.5/f_0$	$\max(14/F_r, 14/f_0)$	$6/f_0$	$\max(14/F_r, 14/f_0)$

Table 3.5 IEEE Std. C37.118 limits for delay time and maximum overshoot during amplitude and phase steps

Test	Delay time (s)		Maximum overshoot	
	P-class	**M-class**	**P-class**	**M-class**
Amplitude/phase steps	$1/(4F_r)$	$1/(4F_r)$	$0.005A_0$	$0.01A_0$

3.5.2 Performance assessment of the i-IpDFT SE algorithm

This section presents a partial performance assessment of the i-IpDFT SE algorithm presented in Section 3.4.2, aimed at demonstrating the improvement introduced by the proposed iterative compensation of the spectral interference produced by the negative image component on the positive frequency range. In particular, this section will analyse the effects of the number of iterations on the estimated synchrophasor accuracy in both static and dynamic conditions by making reference to two test conditions defined in the IEEE Std. C37.118, namely, the *signal frequency* test (see Section 3.5.1.4) and the *system frequency ramp* test (see Section 3.5.1.5).

The reference signals have been synthesized in a software environment where the previously presented i-IpDFT technique has been also implemented. These tests were chosen because they are those in the IEEE Std. [1] that magnify the effects of spectral interference and therefore the tests where the i-IpDFT method should mostly improve the performances of classical IpDFT methods.

The performance of the SE is shown in function of the frequency, amplitude and phase estimation errors as stated in Section 3.5.1.3. In particular, in order to combine multiple plots in a single graph, the simulation results have been presented in a logarithmic scale and therefore the above errors are presented in terms of their absolute value.

3.5.2.1 Steady-state performances

The improvement introduced by the i-IpDFT in steady-state conditions is presented during the signal frequency test (see Section 3.5.1.4) with a nominal frequency of

50 Hz. Nevertheless, equivalent results can be obtained for 60 Hz. The i-IpDFT performances are shown in function of the nominal frequency of each sub-test that, in the case of a 50 Hz power system, must span the frequency interval between 45 and 55 Hz.

In particular, Figure 3.15 shows the maximum frequency, amplitude, and phase errors for various number of iterations (i.e., the parameter r in Algorithm 1), starting from $r = 0$ (i.e., the classical IpDFT approach without any compensation of the spectral interference) up to $r = 4$. The effects of the iterative compensation of the spectral interference produced by the negative image of the spectrum are evident and self-explanatory: the estimation accuracies of frequency, amplitude and phase are improved of almost two orders of magnitude every new iteration, up to the fourth. After, the effects of the spectral interference compensation are no longer visible.

Additionally, it is possible observing that, independently of the number of iterations, the best accuracies are obtained for $f \approx f_0$ (namely for values of frequency closer to 50 Hz) since the effects of spectral leakage interference are here minimized. They deteriorate as the nominal frequency of each sub-test deviates from the rated one f_0 and the effects of spectral interference increase. In particular, the i-IpDFT accuracies are asymmetric with respect to f_0; in other words, the frequency interval on the left of f_0 usually exhibits poorer performances than the frequency interval on the right of f_0. The cause of this behaviour is still related to the spectral interference produced by the negative image spectrum that is higher as the two images get closer, namely for smaller nominal frequencies. Nevertheless, such an asymmetry between the frequency intervals on the left and on the right of f_0 is relative and becomes less and less visible by increasing the number of iterations.

Finally, Figure 3.16 compares the performances of the i-IpDFT SE algorithm with those provided by the classical IpDFT technique that adopt the Hanning window during the signal frequency test. In particular, the five-, four-, three-, and two-period IpDFT SE techniques (dashed lines, various gray scales) are compared to the three- and two-period i-IpDFT SE techniques that adopt four and seven iterations, respectively (continuous lines).

As it can be noticed, the classical IpDFT accuracy is strongly related to the adopted window length and, due to the higher immunity to spectral leakage, the longer the window length the higher the steady-state accuracies. On the other hand, the i-IpDFT technique definitely improves such an accuracy and, at the same time, allows to reduce the window length down to two periods of a signal at the nominal frequency f_0. Such a possibility introduces non-negligible advantages as it allows to considerably reduce the PMU RTs and measurement reporting latencies (see Section 3.5.1.3) without deteriorating the PMU accuracies.

3.5.2.2 Dynamic performances

The improvement introduced by the i-IpDFT technique during dynamic conditions can be evaluated by making reference to the frequency ramp test, defined in the IEEE Std. C37.118 (see Section 3.5.1.5). During this test, the frequency of the reference signal is linearly increased from 45 to 55 Hz at a rate of 1 Hz/s.

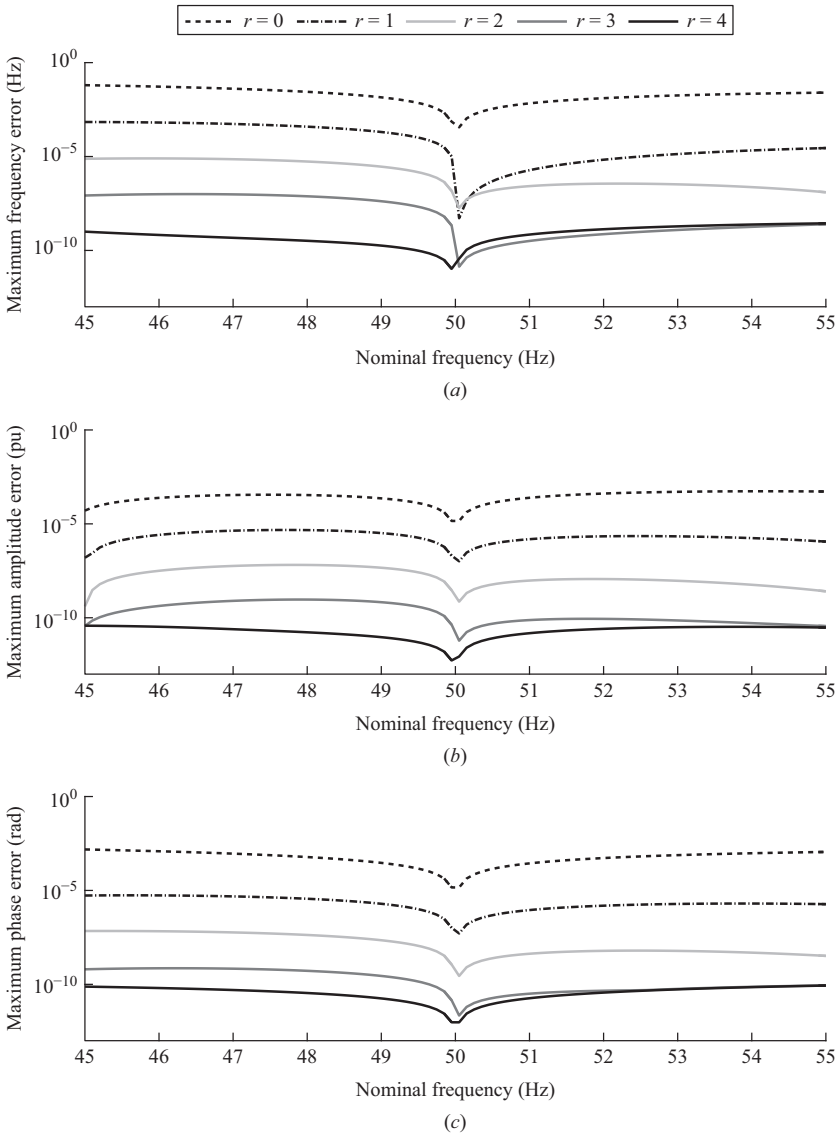

Figure 3.15 Maximum frequency (a), amplitude (b) and phase estimation errors (c) of the proposed i-IpDFT method as a function of the nominal frequency of a steady-state reference signal. The errors are plotted for various number of iterations (r = 0,1,2,3,4), being r = 0 the classical IpDFT method

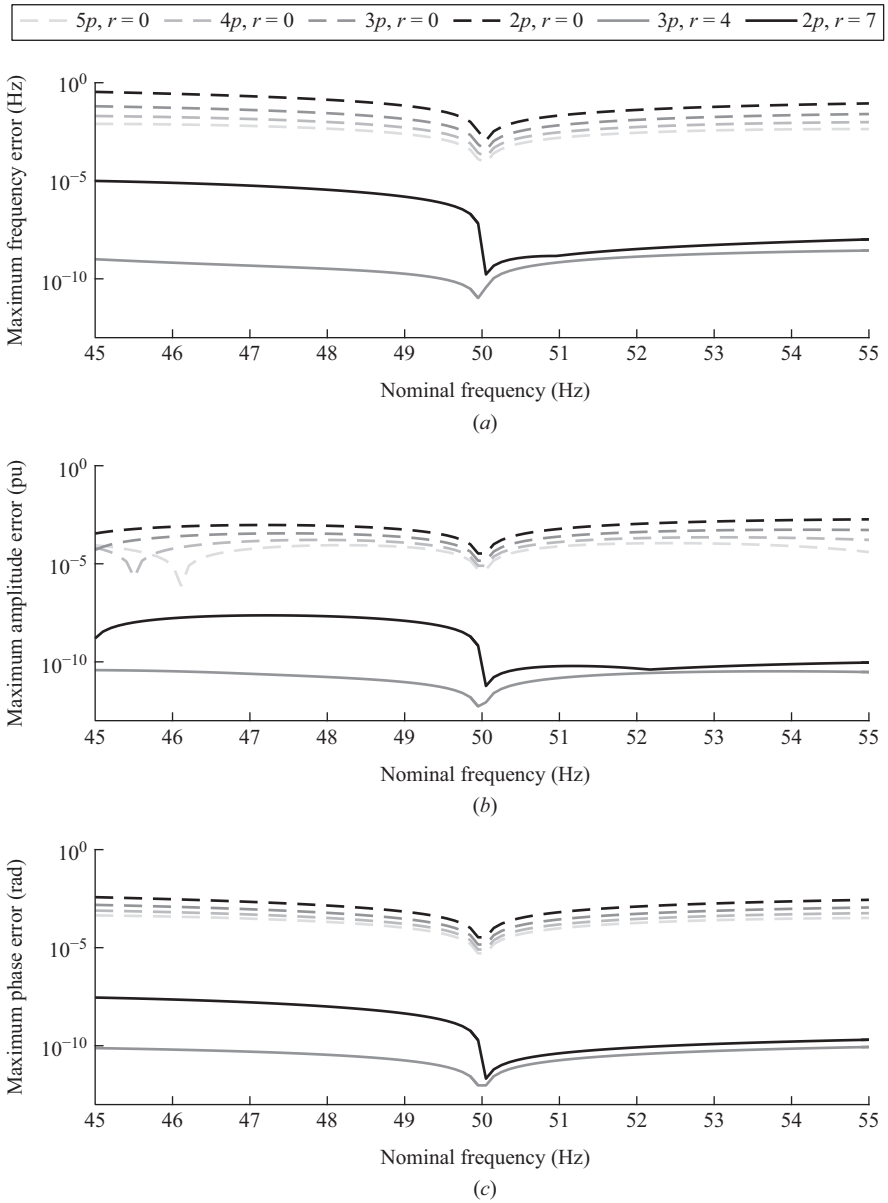

Figure 3.16 Maximum frequency (a), amplitude (b), and phase estimation errors (c) of the proposed i-IpDFT technique versus the classical IpDFT approach. The results are plotted as a function of the nominal frequency of a steady-state reference signal and present, with different gray scales, the results for five-, four-, three- and two-period IpDFT estimators with (continuous) and without (dashed) the proposed iterative compensation of the spectral interference

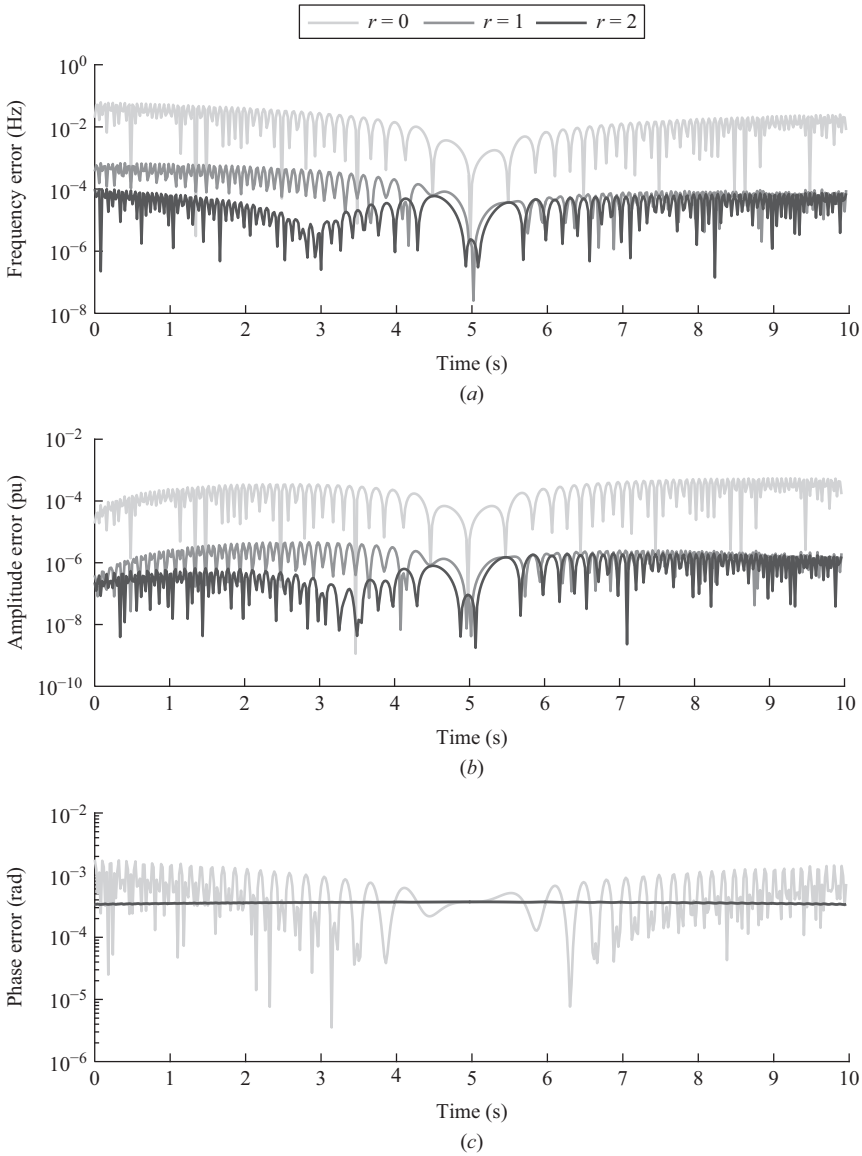

Figure 3.17 Instantaneous frequency (a), amplitude (b), and phase estimation errors (c) of the proposed i-IpDFT technique during a positive ramp of the system frequency. Errors are plotted for various number of iterations (r = 1,2,0), being r = 0 the classical IpDFT method

Figure 3.17 shows the instantaneous errors in the estimation of frequency amplitude and phase during a positive frequency ramp (the results for the negative ramp are here omitted but lead to equivalent conclusions) for various number of iterations. Similarly to the previous figure, the light gray line is obtained for $r = 0$ and makes reference to a classical IpDFT technique where the effects of the spectral interference are neglected. The other two lines are the result of the i-IpDFT with one and two iterations, respectively. Also, during this test, the improvements introduced by the iterative compensation of the spectral interference produced by the negative image of the tone are evident and lead to enhanced accuracies of the estimated synchrophasor that can reach accuracies similar to those obtained during steady state. In particular, the effects of the iterative compensation presented in Section 3.4.2.1 are visible up to the third iteration in the case of the estimated value of frequency and amplitude and up to the second iteration for the estimated phase.

3.6 Conclusions

This chapter has discussed the main elements related to the definition of DFT-based SE algorithms since they represent the most commonly adopted ones in real PMU devices. In particular, this chapter has focused on the analysis of spectral leakage as it represents the most relevant source of uncertainty when using the DFT to estimate the parameters of a sinusoidal signal. This aspect is of importance in SE processes since they usually adopt relatively short windows to reduce the PMU measurement reporting latencies and RTs.

This chapter has also presented state-of-the-art SE algorithms belonging to the family of IpDFT estimators. This chapter has discussed both the classical IpDFT as well as its iterative counterpart (i-IpDFT) capable of dealing with the compensation of the effects of the self-interaction between the positive and the negative images of the spectrum. Such a technique has demonstrated to improve the classical IpDFT performances during both static and dynamic conditions described in the IEEE Std. C37.118 and to be immune to the instantaneous frequency variations of a power system. Furthermore, it has been demonstrated that the i-IpDFT technique outperforms classical IpDFT methods, also by adopting shorter windows (up to two periods) that are usually worsening the estimation uncertainty of any SE algorithm.

Bibliography

[1] IEEE Standard for Synchrophasor Measurements for Power Systems. IEEE Std C37.118.1-2011 (Revision of IEEE Std C37118-2005). 2011; p. 1–61.

[2] Castello P, Lixia M, Muscas C, Pegoraro PA. “Impact of the model on the accuracy of synchrophasor measurement”. *Instrumentation and Measurement, IEEE Transactions on*. 2012 Aug;61(8):2179–2188.

[3] de la Serna JAd. "Dynamic phasor estimates for power system oscillations". *Instrumentation and Measurement, IEEE Transactions on*. 2007 Oct; 56(5):1648–1657.

[4] Castello P, Liu J, Muscas C, Pegoraro PA, Ponci F, Monti A. "A fast and accurate PMU algorithm for P and M class measurement of synchrophasor and frequency". *Instrumentation and Measurement, IEEE Transactions on*. 2014 Dec;63(12):2837–2845.

[5] Bertocco M, Frigo G, Narduzzi C, Muscas C, Pegoraro PA. "Compressive sensing of a Taylor–Fourier multi-frequency model for synchrophasor estimation". *Instrumentation and Measurement, IEEE Transactions on*. 2015 Dec;64(12):3274–3283.

[6] Oppenheim AV, Schafer RW, Buck JR, *et al. Discrete-Time Signal Processing*, vol. 2. Englewood Cliffs, NJ: Prentice-Hall; 1989.

[7] Begovic MM, Djuric PM, Dunlap S, Phadke AG. "Frequency tracking in power networks in the presence of harmonics". *Power Delivery, IEEE Transactions on*. 1993 Apr;8(2):480–486.

[8] Duric MB, Durisic ZR. "Frequency measurement in power networks in the presence of harmonics using Fourier and zero crossing technique". In: *Power Tech, 2005* IEEE Russia; 2005. p. 1–6.

[9] Kamwa I, Leclerc M, McNabb D. "Performance of demodulation-based frequency measurement algorithms used in typical PMUs". *Power Delivery, IEEE Transactions on*. 2004 Apr;19(2):505–514.

[10] Roscoe AJ, Abdulhadi IF, Burt GM. "P and M class phasor measurement unit algorithms using adaptive cascaded filters". *Power Delivery, IEEE Transactions on*. 2013 Jul;28(3):1447–1459.

[11] Roscoe AJ. "Exploring the relative performance of frequency-tracking and fixed-filter phasor measurement unit algorithms under C37.118 test procedures, the effects of interharmonics, and initial attempts at merging P-class response with M-class filtering". *Instrumentation and Measurement, IEEE Transactions on*. 2013 Aug;62(8):2140–2153.

[12] Bertocco M, Frigo G, Narduzzi C. "On compressed sensing and super-resolution in DFT-based spectral analysis". *Proceedings 19th IMEKO TC-4 Symposium and 17th IWADC Workshop Advances in Instrumentation and Sensors Interoperability*. 2013; p. 615–620.

[13] Bertocco M, Frigo G, Narduzzi C, Tramarin F. "Resolution enhancement by compressive sensing in power quality and phasor measurement". *Instrumentation and Measurement, IEEE Transactions on*. 2014 Oct;63(10):2358–2367.

[14] Wong CK, Leong LT, Wu JT, *et al.* "A novel algorithm for phasor calculation based on wavelet analysis". In: *Power Engineering Society Summer Meeting*, 2001. vol. 3. IEEE; 2001. p. 1500–1503.

[15] Guo Q, Zhang C, Shi Y. "Resampling a signal to perform power quality and synchrophasor measurement". Google Patents; 2013. US Patent App. 13/326,676.

[16] de la OS, Antonio J. "Synchrophasor estimation using Prony's method". *Instrumentation and Measurement, IEEE Transactions on*. 2013;62(8): 2119–2128.

[17] Yang L, Jiao Z, Kang X, Wang X. "A novel matrix pencil method for real-time power frequency phasor estimation under power system transients". In: *Developments in Power System Protection (DPSP 2014), 12th IET International Conference on*, Copenhagen, 2014. p. 1–5.

[18] Sidhu TS, Zhang X, Balamourougan V. "A new half-cycle phasor estimation algorithm". *Power Delivery, IEEE Transactions on*. 2005;20(2): 1299–1305.

[19] Phadke A, Thorp J, Adamiak M. "A new measurement technique for tracking voltage phasors, local system frequency, and rate of change of frequency". *Power Apparatus and Systems, IEEE Transactions on*. 1983;(5): 1025–1038.

[20] Warichet J, Sezi T, Maun JC. "Considerations about synchrophasors measurement in dynamic system conditions". *International Journal of Electrical Power & Energy Systems*. 2009;31(9):452–464.

[21] Sachdev M, Nagpal M. "A recursive least error squares algorithm for power system relaying and measurement applications". *Power Delivery, IEEE Transactions on*. 1991;6(3):1008–1015.

[22] Pradhan A, Routray A, Sethi D. "Voltage phasor estimation using complex linear Kalman filter". In: *Developments in Power System Protection, 2004. Eighth IEE International Conference on*, vol. 1. IET; 2004. p. 24–27.

[23] Jain VK, Collins WL, Davis DC. "High-accuracy analog measurements via interpolated FFT". *Instrumentation and Measurement, IEEE Transactions on*. 1979;28(2):113–122.

[24] Grandke T. "Interpolation algorithms for discrete Fourier transforms of weighted signals". *Instrumentation and Measurement, IEEE Transactions on*. 1983;32(2):350–355.

[25] Belega D, Dallet D. "Multifrequency signal analysis by Interpolated DFT method with maximum sidelobe decay windows". *Measurement*. 2009;42(3):420–426.

[26] Paolone M, Borghetti A, Nucci CA. "A synchrophasor estimation algorithm for the monitoring of active distribution networks in steady state and transient conditions". In: *Proc. of the 17th Power Systems Computation Conference (PSCC 2011)*, Stockholm, Sweden, Aug; 2011.

[27] Belega D, Petri D. "Accuracy analysis of the multicycle synchrophasor estimator provided by the Interpolated DFT algorithm". *Instrumentation and Measurement, IEEE Transactions on*. 2013;62(5):942–953.

[28] Belega D, Macii D, Petri D. "Fast synchrophasor estimation by means of frequency-domain and time-domain algorithms". In: *IEEE Transactions on Instrumentation and Measurement*, vol. 63, no. 2, 2014, p. 388–401.

[29] Harris FJ. "On the use of windows for harmonic analysis with the discrete Fourier transform". *Proceedings of the IEEE*. 1978;66(1):51–83.

[30] Andria G, Savino M, Trotta A. "Windows and interpolation algorithms to improve electrical measurement accuracy". *Instrumentation and Measurement, IEEE Transactions on*. 1989;38(4):856–863.

[31] Phadke AG, Thorp JS. "Synchronized phasor measurements and their applications". *Power Electronics and Power Systems*. New York, NY: Springer US; 2008.

[32] Borghetti A, Nucci CA, Paolone M, Ciappi G, Solari A. "Synchronized phasors monitoring during the islanding maneuver of an active distribution network". *Smart Grid, IEEE Transactions on*. 2011;2(1):82–91.

[33] Gunther EW. "Interharmonics in power systems". In: *Power Engineering Society Summer Meeting, 2001*, Vancouver, BC, Canada, vol. 2; 2001. p. 813–817.

[34] IEEE Standard for Synchrophasors for Power Systems. IEEE Std 1344-1995. 1995.

[35] IEEE Standard for Synchrophasor Data Transfer for Power Systems. IEEE Std. C37.118.2-2011 (Revision of IEEE Std C37118-2005). 2011; p. 1–53.

[36] Communication Networks and Systems for Power Utility Automation – Part 90-5: Use of IEC 61850 to Transmit Synchrophasor Information According to IEEE C37.118. IEC TR 61850-90-5:2012. 2012 May.

[37] Castello P, Muscas C, Pegoraro PA. "Performance comparison of algorithms for synchrophasors measurements under dynamic conditions". In: *Applied Measurements for Power Systems (AMPS), 2011 IEEE International Workshop on*; Aachen, 2011. p. 25–30.

[38] IEEE Guide for Synchronization, Calibration, Testing, and Installation of Phasor Measurement Units (PMUs) for Power System Protection and Control. IEEE Std C37242-2013. 2013 Mar; p. 1–107.

[39] Instrument Transformers – Part l: Current Transformers. Int Std IEC 60044-1. 1996.

[40] Instrument Transformers – Part 2: Inductive Voltage Transformers. Int Std IEC 60044-2. 1997.

[41] Papoulis A. *The Fourier Integral and Its Applications. McGraw-Hill Electronic Sciences Series*. New York, NY: McGraw-Hill; 1962.

[42] Cooley JW, Lewis PA, Welch PD. "The fast Fourier transform and its applications". *Education, IEEE Transactions on*. 1969;12(1):27–34.

[43] Darwish HA, Fikri M. "Practical considerations for recursive DFT implementation in numerical relays". *Power Delivery, IEEE Transactions on*. 2007;22(1):42–49.

[44] Jacobsen E, Lyons R. "The sliding DFT". *Signal Processing Magazine, IEEE*. 2003;20(2):74–80.

[45] Douglas S, Soh J. "A numerically-stable sliding-window estimator and its application to adaptive filters". In: *Signals, Systems & Computers, 1997. Conference Record of the Thirty-First Asilomar Conference on*. Pacific Grove, CA, USA, vol. 1. IEEE; 1997. p. 111–115.

[46] Duda K. "Accurate, guaranteed stable, sliding discrete Fourier transform [DSP tips & tricks]". *Signal Processing Magazine, IEEE*. 2010;27(6):124–127.

[47] Romano P, Paolone M. "Enhanced Interpolated-DFT for synchrophasor estimation in FPGAs: theory, implementation, and validation of a PMU prototype". *Instrumentation and Measurement, IEEE Transactions on*. 2014 Dec;63(12):2824–2836.

[48] Nuttall AH. "Some windows with very good sidelobe behavior". *Acoustics, Speech and Signal Processing, IEEE Transactions on*. 1981 Feb;29(1):84–91.
[49] Salih MS, ed. *Fourier Transform: Signal Processing*. InTech, 2012.
[50] Duda K. "DFT interpolation algorithm for Kaiser–Bessel and Dolph–Chebyshev windows". *Instrumentation and Measurement, IEEE Transactions on*. 2011 Mar;60(3):784–790.
[51] IEEE Standard for Synchrophasors for Power Systems. IEEE Std C37118-2005 (Revision of IEEE Std 1344-1995). 2006; p. 1–57.
[52] IEEE Standard for Synchrophasor Measurements for Power Systems – Amendment 1: Modification of Selected Performance Requirements. IEEE Std C371181a-2014 (Amendment to IEEE Std C371181-2011). 2014 Apr; p. 1–25.
[53] IEEE Synchrophasor Measurement Test Suite Specification. IEEE Synchrophasor Measurement Test Suite Specification. 2014 Dec; p. 1–44.
[54] Romano P, Paolone M. "An enhanced interpolated-modulated sliding DFT for high reporting rate PMUs". In: *Applied Measurements for Power Systems Proceedings (AMPS), 2014 IEEE International Workshop on*; Aachen, 2014. p. 1–6.
[55] IEEE Standard Requirements for Instrument Transformers. IEEE Std C5713-2008 (Revision of IEEE Std C5713-1993). 2008 Jul; p. 1–106.